PCCP

Physical Chemistry Chemical Physics

www.rsc.org/pccp

Volume 12 | Number 23 | 21 June 2010 | Pages 5929–6292

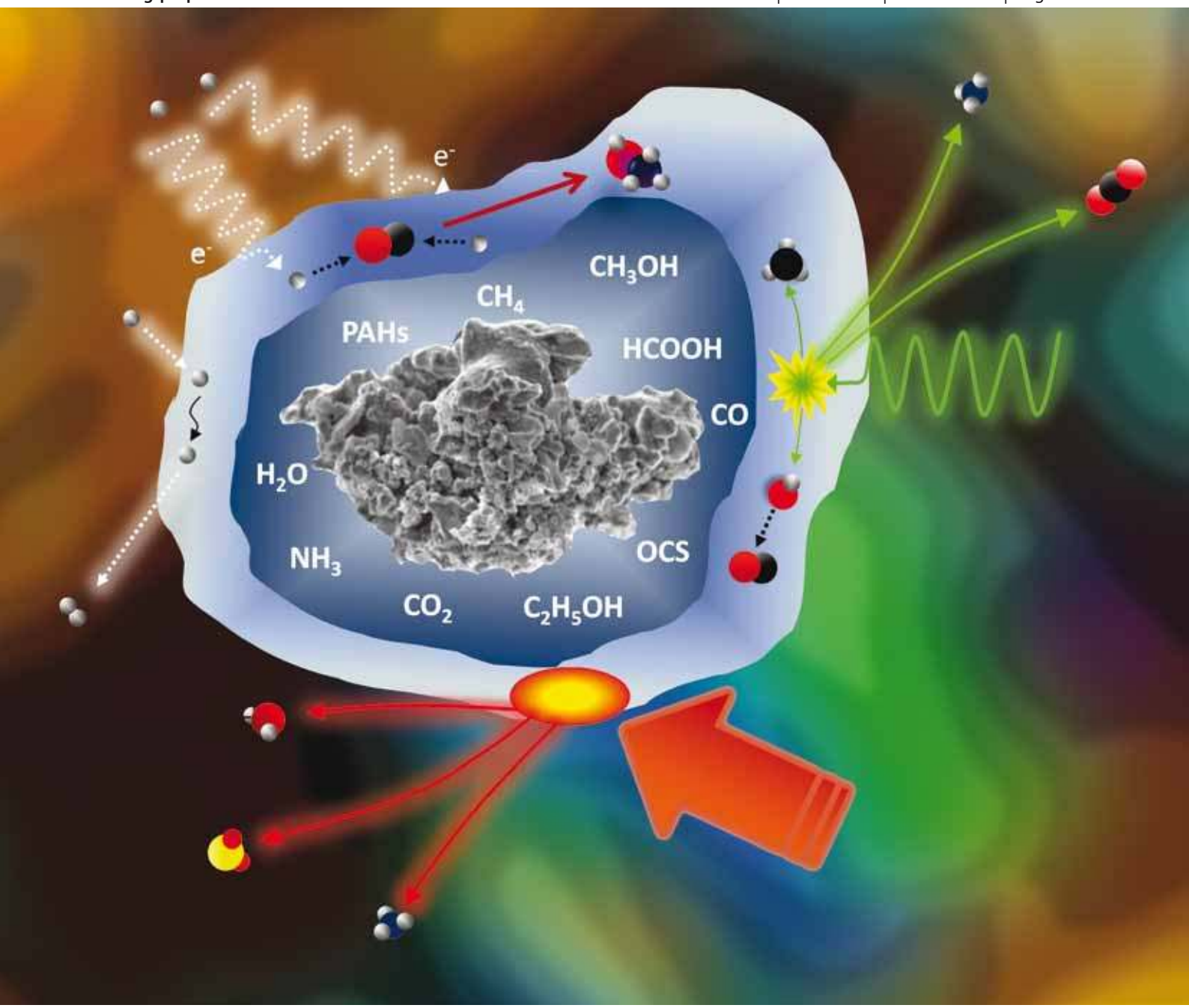

ISSN 1463-9076

1463-9076(2010)12:23;1-0

Ice in space: surface science investigations of the thermal desorption of model interstellar ices on dust grain analogue surfaces

Daren J. Burke† and Wendy A. Brown*

Received 18th August 2009, Accepted 21st January 2010
First published as an Advance Article on the web 23rd February 2010
DOI: 10.1039/b917005g

More than 140 different molecules have been identified in the interstellar medium (ISM) to date. Dust grain particles are also found in the ISM, and some of these molecules freeze out at the cold temperatures (10–20 K) to form molecular ices. Understanding the adsorption and desorption of these ices is crucially important in understanding the processes that lead to star and planet formation, and may even help to lead to an understanding of the origin of life itself. High sensitivity surface science techniques, including temperature programmed desorption (TPD) and reflection absorption infrared spectroscopy (RAIRS), are being increasingly used to investigate the interactions between dust grains and interstellar ices. This perspective provides an overview of the current level of understanding of the adsorption and desorption of astrophysically relevant molecules from a range of dust grain analogue surfaces. Whilst the focus of this review is on interstellar ices, the results discussed are equally valid to discussions of cometary and planetary ices.

1. Introduction

To date astronomers have detected over 140 different molecules in the dense regions of interstellar space known as molecular clouds.[1,2] These range from simple diatomics such as H_2[3,4] and CO[5] to large saturated organics such as $HC_{11}N$.[6] It was initially thought that conditions within these dense molecular clouds, characterised by low temperatures (10–20 K) and pressures (10^4–10^8 hydrogen atoms cm^{-3}), were not conducive to chemistry. However, a combination of infrared, millimetre and microwave spectroscopy has shown that this is not the case and in fact these regions exhibit a rich chemistry and are the birth sites for stars and planets.[7,8]

Over the last 30 years, significant progress has been made regarding the understanding of the formation (and subsequent destruction) of molecules within interstellar space. Current astrophysical models indicate that gas phase chemistry alone cannot account for the variety and richness of molecules observed in star-forming regions. For example, the enhanced abundances of gas phase H_2,[9,10] NH_3,[11] and the presence of alcohols such as CH_3OH[12,13] cannot be explained by gas phase processes. The origin of these enhanced abundances, and the presence of more complex species, is thought to arise from a combination of surface chemistry and the evaporation of "processed" molecular ices that have formed and/or frozen out on the surface of dust grains.[14–20]

Small dust grain nano-particles make up only around 1% of the total mass of the interstellar medium (ISM) but play a

Department of Chemistry, University College London, 20 Gordon Street, London, UK WC1H 0AJ. E-mail: w.a.brown@ucl.ac.uk
† Present address: Laboratory for Atomic and Surface Physics, University of Virginia, Thornton Hall, 351 McCormick Road, Charlottesville, VA 22904-4238, USA.

Daren J. Burke

Daren Burke graduated from the University of East Anglia, where he also obtained his PhD in surface photochemistry on roughened metal surfaces in 2004. After holding research posts at the University of Waterloo and University College London he is currently working as a research associate in the laboratory of Atomic and Surface Physics at the University of Virginia.

Wendy A. Brown

Wendy Brown is currently a Reader in Physical Chemistry at the Department of Chemistry at University College London (UCL), where she has been since 1998. Prior to joining UCL, she held a research fellowship at Peterhouse, University of Cambridge working with the group of Professor Sir David King, in whose group she also studied for her PhD. Her research interests involve studying adsorption and reactions on various surfaces ranging from metals and oxides to model interstellar dust grains.

pivotal role in its chemistry.[21,22] Dust grains are thought to be comprised of silicates, oxides and carbonaceous materials.[23,24] In dense molecular clouds, molecules and atoms from the gas phase condense onto the grains to form molecular ices,[16,21,25,26] the composition of which does not reflect gas phase abundances. During the lifetime of a molecular cloud (10^6–10^8 years) the ices undergo significant physical and chemical changes depending on the astrophysical environment. A summary of some of the typical processing routes for interstellar ices is shown in Fig. 1. The grain acts as a third body, catalysing chemical reactions at the surface. At very low temperatures (<20 K) atomic species such as H, D, N, C and O form simple molecules *via* thermal hopping or quantum tunnelling on grain surfaces.[16] In regions characterised by high atomic H abundances, hydrogenation forms molecules such as H_2O, NH_3, CH_3OH and CH_4.[13,16–19,27] Ices comprised of these molecules are often referred to as polar ices and are dominated by H_2O.[16,28,29] Conversely, in regions where the gas phase atomic and molecular hydrogen ratios are much lower, surface bound C, N and O atoms form so called apolar ices consisting of more volatile species including CO, CO_2, N_2 and O_2.[27,30,31] The presence of multiply deuterated species in the ISM has also been ascribed to grain surface chemistry.[32]

Interstellar ices undergo further processing *via* exposure to ultraviolet (UV),[20,33,34] X-ray or cosmic radiation,[35] in addition to thermal processing. Laboratory studies of ice grain mimics have shown that UV irradiation gives rise to the formation of complex organics such as NH_2CHO, OCN^- and C_2H_5OH.[34,36,37] Bombardment of the ices by low energy protons and ions also leads to the formation of new species, in addition to altering the morphology of the ices.[35,38–41] Heat generated by new born stars stimulates further surface chemistry prior to evaporation of these icy mantles during cloud collapse. In regions of massive star formation known as hot cores, where temperatures rise to in excess of 100 K, sublimation of the ices gives rise to enhanced gas phase abundances of molecules. Once the molecules have been released into the gas phase, they drive a rich chemistry leading to the formation of larger organics such as methyl formate ($HCOOCH_3$) and dimethyl ether ($(CH_3)_2O$).[13,18,42]

Studies have shown that the sublimation of interstellar ices is not instantaneous.[43] Hence a detailed understanding of the thermal desorption of interstellar ices from dust grains is essential for the accurate modelling of star formation. This information can be obtained from surface science techniques such as temperature programmed desorption (TPD) studies of model interstellar ices on dust grain analogue surfaces.[44–57] Numerous studies have shown that the desorption of astrophysically relevant species from H_2O-rich ices occurs over a range of temperatures, instead of a single temperature as assumed in many astrophysical models.[46,48,58–69] Several authors[70,71] have demonstrated the importance of using experimentally determined kinetic parameters to describe the sublimation of interstellar ices from grains. These data can be incorporated into astrophysical models to extrapolate desorption events on timescales relevant to real astrophysical processes. Furthermore, the data can be used to calculate residence times of molecules on grain surfaces as a function of temperature, in addition to providing a more accurate method of estimating total column density (an estimate of the thickness of the ice) in interstellar ices.[55,72,73]

This perspective aims to provide an overview of the current level of understanding of the adsorption, and particularly desorption, of astrophysically relevant molecular ices from a range of dust grain analogue surfaces. Whilst the perspective focuses on the adsorption and desorption of ices in an interstellar context, particularly with respect to star-forming regions and to hot cores, much of the data is equally relevant to discussions of the desorption of cometary and planetary ices, although these are not specifically described here. The main body of the perspective discusses results obtained for a range of different interstellar ices, using ultra-high vacuum (UHV) surface science techniques to study adsorption on and desorption from a range of dust grain analogues. We provide a more general review of some of the experiments that have been undertaken to study ice desorption by several different groups,

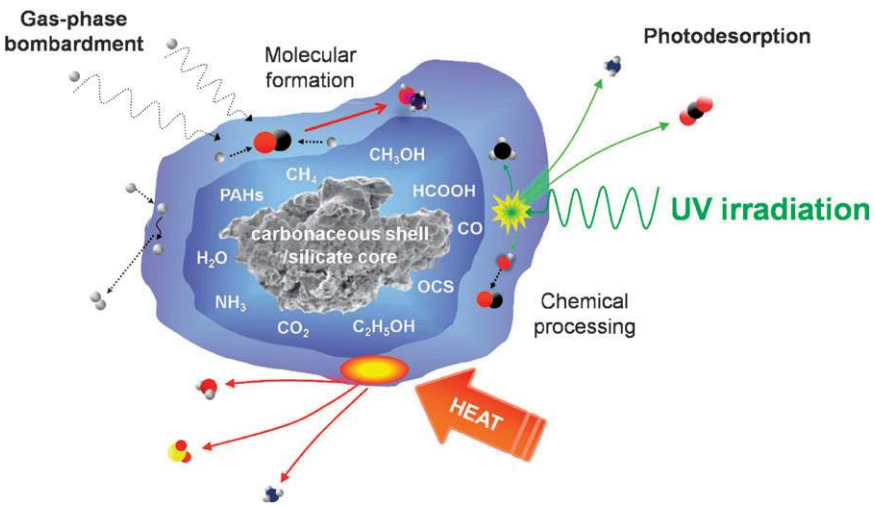

Fig. 1 Schematic showing the main routes of interstellar ice processing that takes place in astrophysical environments. The molecular species labelled within the inner layer highlight the main constituents detected in interstellar ices.

and summarise the kinetic desorption parameters that have been derived for all ice systems studied to date. We then focus in more detail on two important interstellar ice systems—CH_3OH[46,51] and OCS containing ices—using our own data as an illustrative example.

2. Background

2.1 Interstellar dust grains

The exact composition of interstellar dust grains remains a matter of debate. Current knowledge is reliant on the interpretation of visible and UV extinction curves, scattering and polarisation of starlight and measurements of gas phase depletion by UV spectroscopy of nearby stars.[23,24] Advances in interstellar spectroscopy have also made it possible to derive detailed information about the composition and physical nature of the ices frozen out on dust grains.[29,74–76] Spectroscopic observations indicate that dust grains are primarily composed of carbonaceous and silicate materials, ranging in size from 1 nm to 1 μm.[23,24] The carbonaceous material has been ascribed to numerous different forms, including graphite,[77–79] diamond,[80] amorphous carbon,[81] hydrogenated amorphous carbon,[82] coals,[83] polycyclic aromatic hydrocarbons,[84] complex aliphatic carbon chains[85] and organic residues produced by UV photolysis.[86] Silicates also make up a substantial fraction of interstellar dust. Silicate grains are 95% amorphous and are detected near O-rich stars. To a lesser extent, Si–C materials have also been detected.[23]

2.2 Interstellar ice composition

Significant progress in the understanding of interstellar ices has been made since the launch of the Infrared Space Observatory (ISO) in 1995. This instrument enabled astronomers to study interstellar space over the 2.5–45 μm spectral region, allowing the detection of molecules frozen out on dust grains. Stars located behind molecular clouds (field stars) or embedded within the cloud (protostars) provide continuous infrared emission that is absorbed by molecules within the ice. The infrared band profile and peak position is sensitive to ice composition, intermolecular interactions and to the astrophysical environment. Hence information with regard to the chemical and physical evolution of star and planetary systems can be obtained.

The successful interpretation of ISO data has been made by correlating these data with laboratory investigations[34,38,72,87,88] studying interstellar ice analogues under conditions resembling those found in molecular clouds. Fitting data recorded for model interstellar ices to observational infrared data has enabled the unambiguous identification of over 20 molecules in astrophysical ices. A typical infrared absorption spectrum of W33A[76] is shown in Fig. 2. The major constituent of ices in dense molecular clouds is H_2O, making up 60–70% of the ices.[16,28,29] Other major constituents include CH_3OH, CO_2, CO, and to a lesser extent CH_4, NH_3, OCS, HCOOH, CH_2O and OCN^-.[26,74–76,89,90] C_2H_5OH and C_2H_6 have also been detected.[91] The sensitivity of the infrared features (in particular CO and CO_2) to ice composition and temperature have made it possible for astronomers to determine the chemical composition, thermal history and even the presence of distinct layers within interstellar ices.[27,87,92]

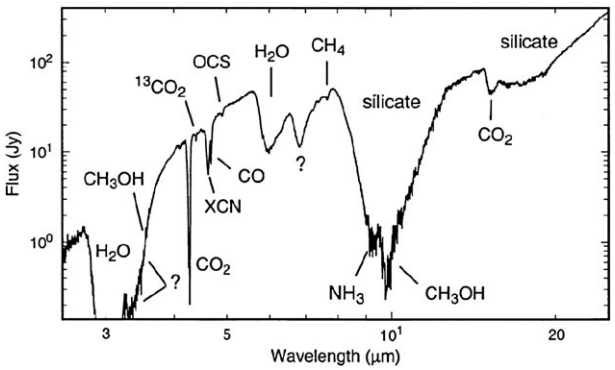

Fig. 2 An ISO spectrum of the embedded stellar object W33A.[76] The spectrum shows the absorption features arising from the components of interstellar ices frozen out on dust grains. The labelled features highlight the main bands that lead to the identification of major constituents of interstellar ices. Reproduced from E. L. Gibb *et al.*, *Astrophys. J.*, 2000, **536**, 347–356. Reproduced by permission of the AAS.

2.3 Laboratory studies on bare dust grain analogues

If accurate data for grain processes are to be derived in the laboratory, then experiments must be performed under astrophysical conditions, using UHV, low temperatures (<20 K), and a suitable model dust grain surface. The nature of the surface is vital in cases where adsorbate–substrate interactions play an important role and where chemical processes depend on binding sites, sticking probabilities, binding energies, desorption kinetics and surface diffusivity. However it is clear from the wealth of information from infrared spectroscopic observations, combined with laboratory work on model grain surfaces and astrophysical ices, that the determination of the exact composition and morphology of dust grains, and the identification of ice constituents, is still ongoing. As a consequence, there is no universal dust grain analogue that can be used in the laboratory.

The question then remains, what constitutes a suitable dust grain analogue that can be used to study gas–grain reactions? Unfortunately there is no immediate solution to this problem, since both grain and interstellar ice composition are strongly dependent on the astrophysical environment. Hence a wide variety of surfaces have been used to investigate astrophysically relevant processes. These include silicates (amorphous and crystalline[93,94]), a variety of carbonaceous surfaces (amorphous carbon,[95] particulate surfaces[96] and highly oriented pyrolytic graphite (HOPG)[51]), metal surfaces[67] (*e.g.* polycrystalline Au, Cu), insulators (CsI),[73] zeolites[97] and also porous films of meteorite[53] and simulated moon dust samples.[98] Furthermore, in dense molecular clouds where the grain is covered in H_2O-rich ices, the ice surfaces themselves must also be studied.[60,67,99]

To date, the primary focus of research on bare dust grain analogue surfaces has been the formation of molecular hydrogen. H_2 is the most abundant molecule in the ISM and plays a key role in many astrophysical processes. It is formed *via* the recombination of hydrogen atoms on bare dust grains in

diffuse clouds.[9,10] Several groups have studied the formation of H_2 and HD *via* the recombination of atomic H/D on a variety of dust grain analogue surfaces.[56,93–95,99–102] The formation of more complex species such as CO_2,[103] H_2O[104–106] and CH_3OH[107–112] has also been investigated, and several reviews have discussed molecular formation on a range of dust grain analogue surfaces.[56,113–116]

In order to produce an analogue more akin to a real dust grain, Mautner *et al*. investigated adsorption on meteorite films.[53] The grain mimic was prepared using laser ablation and controlled condensation techniques under UHV, to create a film of nano-particulate sized fragments deposited on a Au surface. Their preliminary study focused on CO adsorption and desorption and they observed broadened TPD profiles, reflecting the heterogeneity of the surface.[53] The use of novel surfaces has also been extended with the investigation of CO adsorption and desorption on zeolite surfaces.[97]

2.4 Laboratory studies on water ice surfaces

H_2O is a dominant component of many astrophysical ices found in comets, planetary satellites and on interstellar dust.[28,117–120] Hence the interaction of volatile species on and within H_2O-rich ices is of fundamental importance to understanding many interstellar processes. The majority of experiments studying H_2O have focused on the thermal processing of H_2O-rich model interstellar ices. Numerous laboratory studies have shown that the desorption of molecules deposited on the surface of H_2O ice, or co-deposited as an intimate mixture with H_2O, is controlled by the morphology and desorption of H_2O.[46,48,54,58,60–69,88,121–123] H_2O ice exists in a number of different phases, the physical properties of which depend on experimental factors including deposition temperature, the angle of the impinging flux and the method of deposition.[54,124–127] Amorphous solid water (ASW) is the dominant H_2O phase in astrophysical environments[117,120,128–132] and is formed at temperatures below $\sim$130 K. X-Ray and electron diffraction measurements have shown that it exists in two distinct phases.[129,133,134] At low temperatures ($\sim$10 K) a high density amorphous form exists. This undergoes an irreversible phase transition to form a low density, less porous, amorphous phase at 38–68 K.[129] When warmed beyond the glass transition temperature (136 K), ASW transforms into a super-cooled metastable liquid, prior to crystallisation at 160 K.[135,136] The change in porosity and surface area of the ice during the ASW–CI (crystalline ice) transition can result in the trapping or release of volatile species deposited on or within the ice.[137] CI has also been detected within many astrophysical environments[138–140] and is formed as a result of thermal processing[141] or during the condensation stage within circumstellar envelopes of evolved stars.[128,138] A further stable form of ice (hexagonal ice) is formed at temperatures above 170 K, and has a structure more associated with terrestrial conditions.

The porosity of ASW has been probed by studying the adsorption and desorption of a variety of molecules on H_2O-ice surfaces.[99,124–127,142–146] TPD[125,127] and electron stimulated desorption[142] measurements of N_2 desorption from ASW films have shown the surface to be highly porous. The porosity of ASW and the ice phase can be controlled by the deposition angle,[125,127] deposition temperature, and by the thermal history of the ice and substrate.[142] Using a combination of experiment and theory, it has been shown that ASW has dangling bonds[143,144,147,148] at the surface that provide preferential sites for molecular adsorption.[143,149] An examination of the desorption kinetics of various molecules (H_2, D_2, N_2, CH_4) from ASW has also provided insight into the porosity of ASW films, demonstrating a range of binding sites at the surface.[127,146] The porous ASW ice surface catalyses several key surface reactions which are particularly relevant to the ISM. In particular, the catalytic effects of the ASW surface have been investigated for H_2 formation.[99–101] ASW has also been shown to catalyse the formation of CH_3OH.[108,109]

Several publications have also highlighted the role of H_2O ice in the UV and cosmic ray processing of interstellar ices.[34,36,88,150,151] The formation of CO_2,[150] CH_3OH[88,152] and C_2H_5OH,[37] in addition to other complex species, has been reported in multi-component ices.[34] In these experiments, the substrate was not considered an important factor. However, recent experiments have shown that the surface can provide an additional route of energy transfer following photon absorption, leading to the formation or photodesorption of molecules from interstellar ices.[153] Ion bombardment of mixed interstellar ice mimics has also shown an alternative route to the formation of simple molecules such as CO_2 from pure CO ice films[39] and more complex organics from H_2O/CO ices.[154]

Clearly, studies of the thermal desorption of interstellar ice mimics are extensive and have been performed on a wide variety of surfaces. However, in many cases parameters that accurately describe the desorption kinetics of astrophysically relevant molecules adsorbed on dust grain surfaces have not been fully characterised. In the following, the adsorption and desorption of several astrophysically relevant volatiles on a range of dust grain analogue surfaces will be described.

3. Experimental techniques

To fully understand surface adsorption and desorption on model interstellar dust grains requires a combination of scientific disciplines, including astronomy, chemistry, physics and surface science. It also requires the use of state-of-the-art apparatus, used to mimic the conditions of the ISM. Most experiments are performed in an UHV apparatus with a base pressure of $\leq 2 \times 10^{-10}$ mbar. In this case, the major constituent of the vacuum in the chamber is H_2, providing similar conditions to those found in the ISM.

The two main techniques used to study adsorption and, more specifically, thermal desorption are infrared spectroscopy and TPD. Infrared spectroscopy has been used in both the reflection mode (reflection absorption infrared spectroscopy—RAIRS), as used by ourselves and by McCoustra and co-workers,[48,53,66,155,156] and in the transmission mode as in the experiments of Sandford and Allamandola[72,73,157–160] and Gálvez *et al.*[54] Infrared spectroscopy is a fingerprinting technique that can be used to identify the nature of the adsorbate on the model grain surface (physisorbed, chemisorbed *etc.*) and to give information about any interactions between the adsorbate and co-adsorbates such as H_2O-ice. On metallic and semi-metallic

model grain surfaces, such as graphite, RAIRS can also be used to give information about the orientation of the adsorbate, by using the metal surface selection rule to identify the number of allowed vibrational modes for a given adsorbate orientation. Transmission infrared spectroscopy has also been used to determine desorption activation energies for a wide range of model interstellar ices (see later) by monitoring the decrease of the integrated absorbance of infrared bands as a function of annealing time and temperature.[54,72,73,157–160]

TPD is a mass spectrometric technique that has been used by several groups[46–48,50–52,57,58,60–62,64,66,67,69,122,123,161,162] to monitor the desorption of model interstellar ices as a function of annealing temperature. TPD is particularly useful, as not only can the nature of the desorbing species be identified from its mass, but detailed analysis of TPD data recorded as a function of coverage, such as that presented in Section 4.3, can be used to determine the kinetic parameters that govern desorption.

In our own experiments, reported in Section 4, the dust grain analogue is highly oriented pyrolytic graphite (HOPG). HOPG is considered a suitable dust grain analogue surface and has been widely used to investigate the formation of simple molecules, such as H_2 and HD.[56,102,163] HOPG has the advantage of being easy to clean and maintain under UHV conditions. The ordered structure of the surface and its derivatives (such as graphene) also make it a useful model grain surface for theoretical investigations of catalytic processes in the ISM.[164–168]

To model the low temperature conditions of the ISM, the dust grain analogue must be cooled to 10–20 K. This is usually achieved by mounting the sample on the end of a closed cycle He refrigerator, as in our experiments, or on the end of a liquid He cooled cryostat. Experiments have also been performed using liquid nitrogen sample cooling, giving sample temperatures of around 90 K.

A range of different methods of dosing are used to grow model interstellar ices *in situ*. Typically, gases are admitted into the UHV chamber *via* a high-precision leak valve, which either fills the whole chamber with the dosing gas or doses the gas of choice *via* a directional doser pointing directly at the sample. The latter is preferable as it avoids the dosed gases freezing out on all of the cold surfaces in the chamber. Doses are usually measured in Langmuir (L), as in our experiments, where 1 L = 10^{-6} Torr s. Ice thicknesses are estimated using various methods, the most accurate of which is a quartz crystal micro-balance.[156] In our own experiments, ice thicknesses were estimated from a knowledge of the dosing rate and were found to range from monolayers at the lowest exposures (3 L) to around 50 Å thick multilayers for the thickest ices (300 L).

4. Results and discussion

A wide range of studies of surface processes of relevance to interstellar space have been performed, in many different laboratories. These include studies of molecular formation,[102,112,116,163] studies of UV[34,37,88,152,169–171] and electron[172,173] irradiation of interstellar ices, and studies of the ion bombardment of interstellar ices.[39,40,154,171,174–176] This perspective focuses on investigations of the adsorption and, more importantly, thermal desorption of model interstellar ices. Thermal desorption studies that specifically address astrophysical problems have been published by numerous research groups. In the following, examples will be used to illustrate how surface science techniques can be employed to provide a detailed picture of the thermal behaviour of cometary and interstellar ices. This is not intended to be an exhaustive review, but aims to inform the reader of the ice systems studied to date and the primary techniques used to study them. This will be followed by a more detailed discussion of two important model ice systems—CH_3OH[46,51] and OCS containing ices adsorbed on a carbonaceous model grain surface (HOPG)—using our own work as an illustrative example of the type of information that can be obtained for these systems. CH_3OH, CH_3OH/H_2O layered ices and CH_3OH : H_2O mixtures are typical of molecules detected within polar ices and will be used to illustrate the general trends seen for astrophysically relevant molecules exhibiting hydrogen bonding. New data for OCS desorption from HOPG, from ASW ices and from OCS : H_2O mixtures will be presented to illustrate the trends observed for non-hydrogen-bonded species, often detected within non-polar ices.

4.1 Overview of the thermal desorption of model interstellar ices in the laboratory

As indicated previously, laboratory studies cannot exactly reproduce astrophysical conditions. Difficulties in identifying a suitable dust grain analogue remain a key issue. The multi-component nature of interstellar ice also adds to the complexity of experiments. Furthermore, heating rates are clearly constrained on a laboratory timescale, compared to those observed under astrophysical environments. The question then arises, what can UHV and surface science provide with regard to understanding the thermal processing of interstellar ices?

Several investigations have focused on infrared and TPD studies of the adsorption and desorption of pure ices adsorbed on a variety of substrates.[47,50–52,57,72,73,92,157–160,177] At first glance such experiments do not seem astronomically relevant, since interstellar ices are multi-component in nature. However, the study of pure molecular ices provides a firm foundation to aid the understanding of the adsorption and desorption of more complex ices such as those observed in the ISM.

Collings and co-workers[67] have studied the desorption of a wide variety of astrophysically relevant molecules in an astronomical context. Fig. 3 shows TPD spectra for a range of molecular ices adsorbed on polycrystalline Au at 8 K.[67] The data illustrate the wide range of desorption temperatures and desorption characteristics observed for each species. These range from highly volatile species such as CO, O_2, N_2 and CH_4, which desorb at temperatures <30 K and clearly show monolayer and multilayer desorption, to larger molecules such as CH_3OH and HCOOH that are characterised by much higher sublimation temperatures and more complex desorption behaviour.

Typically, data have shown that astrophysically relevant adsorbates are weakly bound to metallic, graphitic and silicate surfaces, forming physisorbed multilayer ices.[47,50–52,57,177] Furthermore, TPD data for a range of substrates can be compared, to determine whether the substrate plays a significant

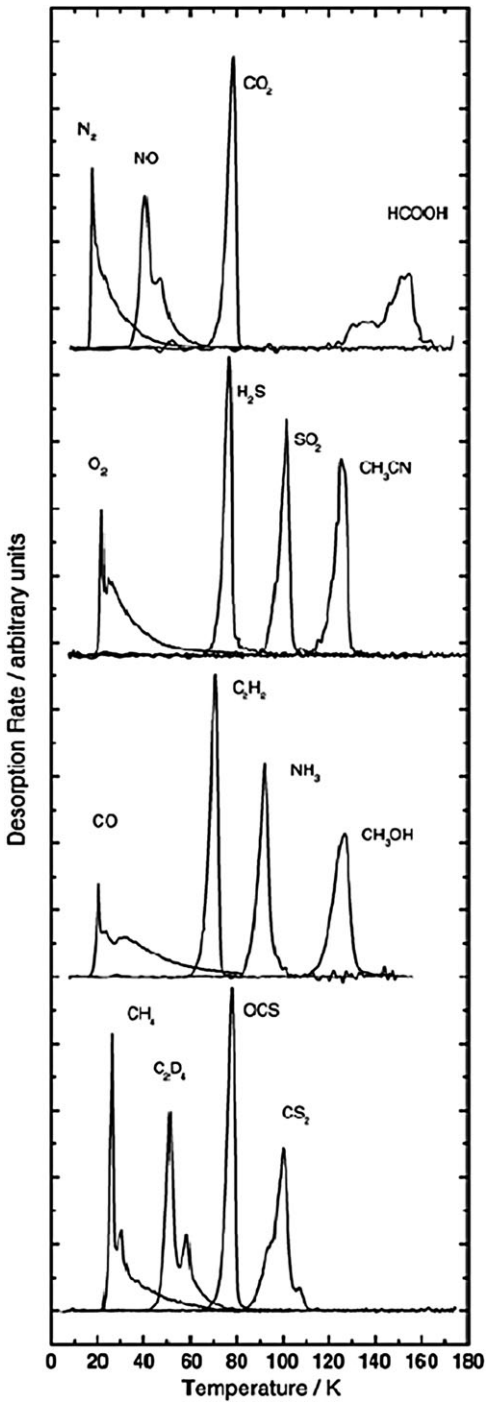

Fig. 3 TPD traces of various astrophysically relevant species deposited on a bare gold substrate at 8 K. Each trace has been arbitrarily scaled such that the total desorption yield is equal. TPD experiments were performed using a constant heating rate of 0.08 K s^{-1}. Reproduced from M. P. Collings *et al.*, *Mon. Not. Astron. Soc.*, 2004, **354**, 1133–1140, John Wiley and Sons. Reproduced with permission.

role in dictating the desorption kinetics of astrophysically relevant ices. Such a study was recently performed by Green *et al.* who compared the thermal desorption of pure CH_3OH ices grown on graphitic (HOPG),[51] amorphous silica and polycrystalline Au substrates.[177] Examination of the desorption data from different substrates indicated that at higher surface coverages, CH_3OH desorption was independent of the underlying substrate, as expected. Substrate dependent desorption was however observed at lower coverages. However, the size distribution of the dust grains and variations in the heating rate were found to be more significant than the nature of the substrate in modifying desorption kinetics.

The most useful information gleaned from the study of pure ices is the determination of the desorption kinetics[44,45,47–52,54,57,72,73,157–160,178] of the ices. Kinetic data have been reported for a range of astrophysically relevant molecules using infrared[54,72,73,157–160] and TPD techniques[44,45,47–53,57,178,179] and these data are summarised in Tables 1–3. Sandford and co-workers determined binding energies for a range of astrophysically relevant molecules using infrared transmission spectroscopy.[72,73,157–160] Surface binding energies were determined by monitoring the decrease of the integrated absorbance of spectral features of the ice as a function of annealing time. Measurements have been reported for a range of pure ices deposited on CsI at 10 K, including H_2O, CO, CO_2 and NH_3 ices, in addition to CO_2, CO and H_2 desorption from H_2O ices (Table 1). More recently Gálvez *et al.* employed a similar technique, using infrared spectroscopy, to describe the desorption of CO_2 from amorphous and annealed H_2O ices.[54]

In the majority of cases, however, TPD has been employed to measure the desorption kinetics of astrophysically relevant molecules. Numerous methodologies have been derived in order to extract desorption kinetics from TPD curves.[180] TPD curves can be described by the Polanyi–Wigner equation.[181] Leading edge analysis of a series of TPD curves can then yield kinetic parameters, such as desorption orders, desorption energies and pre-exponential factors for pure ices. This methodology is used in our laboratory to determine the desorption kinetics of astrophysically relevant molecules[50–52,57] and is described later. An alternative approach has been used by Fraser *et al.*[47] to determine the parameters for the desorption of H_2O ices (and later of CH_3OH[177] ices and for CO desorption from ASW films[48]). Desorption energies and pre-exponential factors are determined from the solution of a set of differential equations that describe the thermal desorption of the ice, and the pumping rate of the UHV system. The unknown kinetic parameters are varied until a

Table 1 Desorption energies for astrophysically relevant ices, derived using infrared absorption spectroscopy (see references for details of the methods used). In all cases, the assumed desorption order is 1

Molecule	Substrate	Desorption energy/kJ mol^{-1}
SO_2[159]	CsI	28.8 ± 0.3
CO_2[72]	CsI	22.4 ± 1.2
CO_2[54]	H_2O (ASW)	21 ± 2
CO_2[54]	H_2O (CI)	20 ± 2
CO_2[72]	H_2O	23.8 ± 1.2
CO[73]	CsI	7.9 ± 0.1
CO[72]	H_2O	14.5 ± 0.4
H_2O (unannealed)[73]	CsI	40.0 ± 0.1
H_2O (annealed)[73]		42.1 ± 0.4
CH_3OH[157]	CsI	35.2 ± 0.1
NH_3[157]	CsI	25.6 ± 0.2
H_2[160]	CsI	1.9
H_2[160]	H_2O	4.6 ± 0.3

Table 2 Kinetic parameters for the desorption of multilayers of pure ices from a range of astrophysically relevant model ices, derived using TPD spectroscopy

Molecule	Substrate	Desorption order	Desorption energy/kJ mol^{-1}	Pre-exponential factor/molecules m^{-2} s^{-1}
H_2O[178]	HOPG	0	46 ± 3	$9 \times 10^{14\pm1}$ [a]
H_2O[47] (ASW)	Au	0	46.6 ± 0.5	1×10^{30}
H_2O[47] (CI)	Au	0	47.9 ± 0.5	1×10^{30}
CH_3OH[178]	HOPG	0	46 ± 3	$3 \times 10^{16\pm2}$ [a]
CH_3OH[177]	Au	0	43.2 ± 0.9	$3 \times 10^{30\pm1}$
CH_3OH[177]	Silica	0	45.4 ± 0.9	$3 \times 10^{30\pm1}$
CH_3OH[179]	Al_2O_3	0	46.4 ± 2.1	3×10^{24}
C_2H_5OH[178]	HOPG	0	46 ± 3	$2 \times 10^{15\pm2}$ [a]
NH_3[178]	HOPG	0	25 ± 2	$5 \times 10^{13\pm1}$ [a]
CO_2[178]	HOPG	0	23 ± 2	$6 \times 10^{14\pm1}$ [a]
CO[178]	HOPG	0	13 ± 1	$2 \times 10^{14\pm1}$ [a]
CO[44,45]	Au	0	7.1 ± 0.1	$7 \times 10^{26\pm1}$
CO[53]	Meteorite	1	13.5 ± 3	10^{13} [b]
CO[48]	H_2O	0	9.8 ± 0.2	—
O_2[44,45]	Au	0	7.7 ± 0.2	$7 \times 10^{26\pm1}$
N_2[44,45]	Au	0	6.6 ± 0.2	$7 \times 10^{26\pm1}$

[a] Note that these pre-exponential factors are first order values, despite the quoted desorption order of zero. [b] This is a real first order pre-exponential factor, with units of s^{-1}.

match is found between experimental and simulated data. The advantage of this method is that it can be applied for non-linear heating rates, and additional desorption steps for more complex desorption schemes can also be incorporated.[48] However, this method requires an accurate knowledge of the surface coverage and an assumption of the desorption order in order to undertake the simulations.

Studies of the desorption of astrophysically relevant molecules adsorbed on ASW have also been performed. Understanding the adsorption and desorption of astrophysically relevant volatiles deposited on ASW ices is equally, if not more, important as investigating desorption from bare grain analogues. Although interstellar ices usually form complex mixtures, highly volatile species such as CO, N_2 and CH_4 are thought to be formed *via* gas phase chemistry and they accrete onto the surfaces of interstellar icy mantles at low temperatures (<20 K). Interstellar ices undergo significant desorption and re-adsorption, and hence the investigation of layered binary ices, where adsorbates are deposited on top of (or beneath) ASW, is relevant to the ISM and to cometary environments. As a result, several groups have studied the interaction of astrophysically relevant molecules with ASW surfaces using a combination of infrared and TPD spectroscopies.[46,48,54,60,63,65–69]

Ayotte *et al.* investigated the adsorption, trapping, and release of 5 highly volatile species deposited on dense and porous ASW films at 22 K.[65] Controlling the surface porosity of the ASW film, by changing the angle of the impinging flux during deposition, demonstrated how ASW ices control the sublimation behaviour of all of the adsorbates. Fig. 4 (left panel) shows the desorption of 1 monolayer (ML) of Ar, CH_4, CO, N_2 and O_2 from dense ASW films. Desorption of all of the adsorbates occurred below 60 K, at temperatures resembling those observed for the pure ices investigated by Collings *et al.*[67] (Fig. 3). Fig. 4 (right panel) shows the corresponding desorption profiles for the same species from porous ASW films. Desorption from the porous ASW ices below 80 K accounts for 95% of the deposited ice. However, desorption is also observed in two additional high temperature peaks that are common for all of the adsorbates investigated.

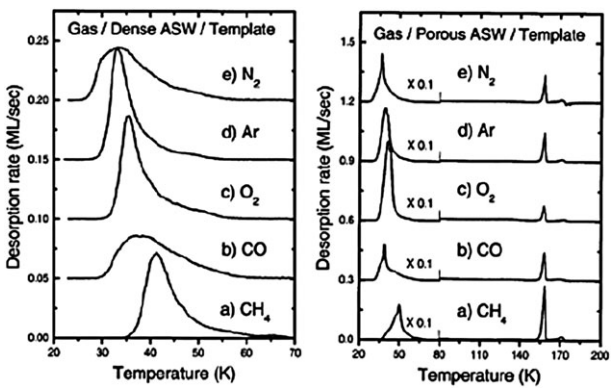

Fig. 4 TPD spectra for (a) CH_4, (b) CO, (c) O_2, (d) Ar and (e) N_2 deposited on top of dense (left panel) and porous (right panel) ASW at 22 K. The spectra below 80 K for porous ices are multiplied by a factor of 0.10 to keep both low and high temperature features on the same scale. Reproduced from P. Ayotte, R. S. Smith, K. P. Stevenson, Z. Dohnalek, G. A. Kimmel and B. D. Kay, *J. Geophys. Res. Planets*, 2001, **106**, 33387–33392. Copyright (2001) American Geophysical Union. Reproduced by permission of American Geophysical Union.

The appearance of the two additional high temperature features in the TPD spectra and the modification of the low temperature desorption for these volatile molecules on porous ASW can be explained by Fig. 5. The figure illustrates the desorption of CO deposited on ASW at 8 K.[66] This general trapping and release mechanism is also representative of that observed for other volatile molecules, including O_2, N_2 and CH_4. Briefly, at temperatures <70 K desorption competes with surface diffusion. Between 15–30 K, multilayer CO desorbs at the same time as it diffuses into the pores of ASW. As the temperature rises, CO desorbs from the surface. The increased surface area generated by the heterogeneity of the porous ASW film gives rise to a range of different binding sites[127,146,182] and to an increased capacity of the water surface for adsorption,[65,125,127] which yields a modified desorption profile for monolayer CO (as seen in the right hand panel of Fig. 4). At temperatures between 30–80 K, ASW undergoes a

phase transition leading to partial pore collapse and entrapment of CO. At 140 K, CO desorption occurs abruptly *via* a volcano desorption mechanism.[137] Here ASW converts to CI, leading to the formation of connected pathways to the surface that allows some of the trapped CO to escape. The characteristics of this desorption are dependent on the crystallisation process, which in turn depends on the heating rate. Finally CI desorbs from the surface, allowing the release of the remaining trapped CO.

TPD experiments using simple two-component mixtures dominated by H_2O are often studied in concert with studies of layered ices[54,60,66,68,69] to provide a more complete picture of the desorption dynamics of model interstellar ices. These co-deposited ice systems are more astrophysically relevant compared to layered ices as they more closely represent the structure of real interstellar ices.

BarNun and co-workers have extensively investigated two-component and multi-component ice mixtures using a wide range of astrophysically relevant molecules, from volatile species, such as H_2, CO, N_2 and CH_4, extending up to complex molecules such as CH_3OH and n-C_6H_{14}.[58,60–62,64,122,123,161,162] These experiments have illustrated the key factors that govern

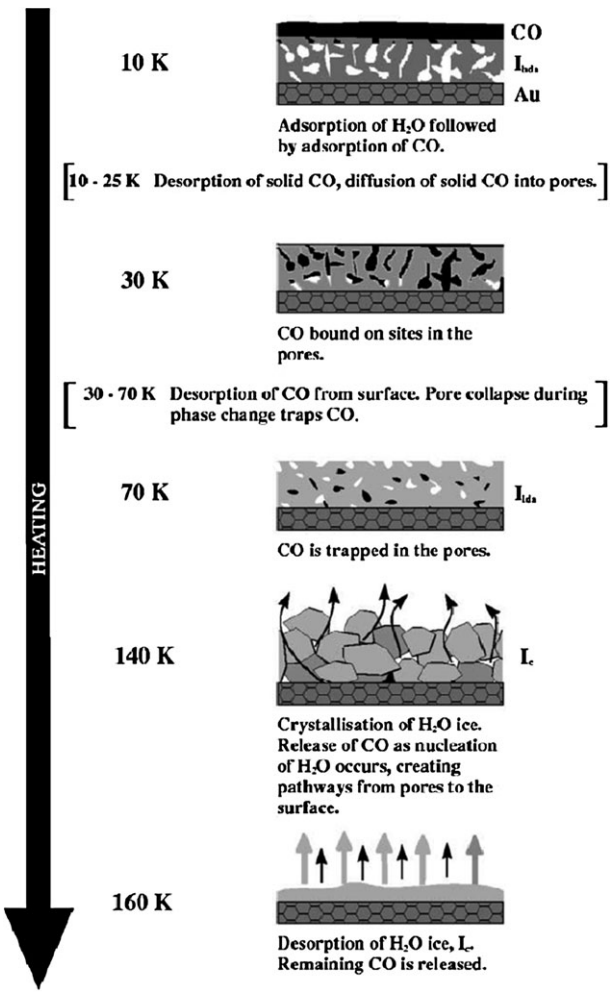

Fig. 5 Cartoon summarising the behaviour of CO adsorbed on amorphous H_2O under laboratory conditions (not to scale). Reproduced from M. P. Collings *et al.*, *Astrophys. J.*, 2003, **583**, 1058–1062. Reproduced by permission of the AAS.

the trapping efficiency of ASW and the sublimation behaviour of the trapped gases from model cometary and interstellar ices. Fig. 6 (left panel) shows thermal desorption spectra for a co-deposited 4-component mixture containing H_2O, CH_4, CO and Ar deposited on CsI at 50 K.[62,123] Gases desorb from the H_2O-rich ice over 8 different temperature ranges. However, the desorption of the volatile components of the mixture can be simplified into two main steps, analogous to the behaviour observed for sequentially deposited systems. At low temperatures, multilayer and monolayer desorption from the surface of the mixed ice is observed (regions b + c). This is followed by more complex high temperature (T > 135 K) desorption arising from the trapped component of the gas, released as a result of structural changes in the H_2O ice (regions d–f).

Fig. 6 (right panel) shows a plot of the volume of trapped gas as a function of deposition temperature for binary mixtures of H_2O ices co-deposited in a 1 : 1 ratio with CO, N_2, Ar and CH_4 and for a complex mixture of H_2O : CH_4 : Ar : CO (or N_2). The plot provides a summary of several competing factors, and shows that the trapping behaviour of ASW is dependent on both the morphology of the ASW ice and on the properties of the trapped gases. Clearly the trapping efficiency is dependent on the porosity of ASW, which in turn is dependent on the deposition temperature of the ice. The amount of trapped gas decreases exponentially as the deposition temperature increases from 24 to 100 K. This is in part due to the number of trapping sites available within the ASW ice, which decreases as it converts from high density to low density amorphous ice and then to CI. However, the higher deposition temperatures also show that the trapping depends on the properties of the gas. At the lowest temperature, 24 K, all gases are trapped equally. At temperatures between 50–75 K, CH_4 is preferentially trapped over CO, N_2 and Ar. Factors such as sublimation temperature,[58,64] molecule/atom size[61,62,64,123] and the strength of interaction of the atom/molecule with H_2O[62,64] have all been found to play a significant role in the trapping mechanism. For example, CO traps more efficiently than N_2 due to its larger dipole moment, and hence stronger interaction with H_2O.[58] Furthermore the strong interaction that exists between CH_3OH and H_2O and its relatively high sublimation temperature accounts for the high trapping efficiency of CH_3OH in ASW.[64]

In contrast to TPD, infrared spectroscopy provides a useful tool to probe the state of model interstellar ices upon adsorption and during the heating process. The sensitivity of infrared absorption bands to ice composition and temperature make it an ideal technique to study the composition of model interstellar ices. An extensive range of mixed ices have been studied in the laboratory and have been used to interpret astronomical spectra with regard to the ice composition, relative abundances and thermal history of ice films.[30,72,73,85,91,92,157–160,183–185]

Sandford and Allamandola studied the properties of CO_2 as a function of temperature and ice composition in pure, binary and tertiary ice mixtures using infrared transmission spectroscopy.[158] Fig. 7 shows the change in the CO_2 ν_3 band in pure CO_2, binary H_2O : CO_2 (20 : 1) and tertiary H_2O : CH_3OH : CO_2 (20 : 10 : 1) mixed ices adsorbed on CsI at 10 K. At 10 K, pure CO_2 ice exhibits a broad infrared band centred at $\sim$2343 cm^{-1}, with a high frequency shoulder.

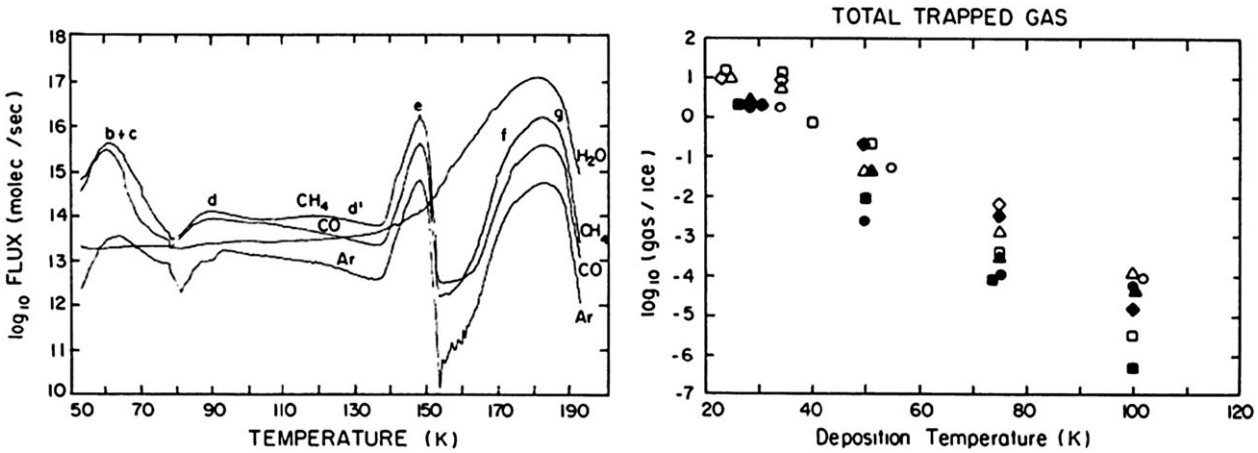

Fig. 6 Left panel: thermal desorption spectra showing the evolution of gas from a H_2O : CH_4 : CO : Ar (1 : 0.33 : 0.33 : 0.33 : 0.33) ice mixture condensed at 50 K. Right panel: total amount of trapped gas as a function of deposition temperature. (◇) CH_4, (△) CO, (○) N_2, and (□) Ar. Open symbols represent a 1 : 1 gas : water mixture. Solid symbols represent a H_2O : CH_4 : Ar : CO (or N_2) mixture. Some points are shifted on the temperature axis to prevent overlap. Reprinted (figures) with permission from A. Bar-Nun, I. Kleinfeld and E. Kochavi, *Phys. Rev. B: Condens. Matter*, 1988, **38**, 7749–7754. Copyright (1988) by the American Physical Society.

The high frequency feature is not evident in the mixed ices and is attributed to CO_2–CO_2 interactions, which are clearly inhibited in the mixed ices. Furthermore, the peak profile, position and width of the CO_2 ν_3 band clearly varies in all three ices at 10 K, with an increasingly narrower peak width and shift to lower frequency observed for the H_2O : CO_2 and H_2O : CO_2 : CH_3OH ices respectively. This distinctive behaviour for all three ices is also observed during annealing. Experiments clearly demonstrate that CO_2 remains trapped within the mixed ices beyond its normal sublimation temperature, as reported in several TPD studies.[54,67,68] However, it is also clear that the presence of CH_3OH in the ice gives rise to significantly modified thermal behaviour compared to the binary system. At 140 K, the CO_2 ν_3 band at 2340 cm^{-1} is characterised by a significant decrease in intensity, coupled with the development of a new band near 2346 cm^{-1}. It has been proposed that CH_3OH is incorporated into the crystalline structure of the annealed ice giving rise to a larger number of available sites that could retain CO_2. Similar observations have also been reported for CH_3OH doped ices in other experiments.[161,186,187] These experiments provide important information with regard to the ice composition and thermal history of interstellar ices for comparison with astronomical infrared data.

Although not intended to be comprehensive, the summary given above gives an idea of some of the information that can be gained using a range of UHV surface science techniques to study the adsorption, and most importantly the desorption, of model interstellar ices. We now focus on two important ice systems: CH_3OH and OCS containing model interstellar ices, in order to discuss in detail some of the data obtained for model interstellar ices. In both of these cases, we use our own data to illustrate what is currently known about these systems.

4.2 Adsorption and desorption of CH_3OH containing interstellar ices

CH_3OH is the most commonly detected molecule within interstellar ices after H_2O[188,189] and has received considerable attention in the astrophysical literature.[46,51,64,157,161,177,184,185,190,191] It has been detected within polar and apolar ices with abundances varying considerably depending on the astrophysical environment. The abundance of CH_3OH has been estimated to be as low as 5% with respect to H_2O in dark molecular clouds, rising to 15–30% in the vicinity of low[192] and high mass protostars.[188,189,193] Laboratory studies of model interstellar ices suggest that CH_3OH is closely associated with H_2O and CO_2, forming CO_2–CH_3OH complexes, prior to segregating into pure CH_3OH ices before outgassing.[184,185,190,194] It is now widely acknowledged that the majority of CH_3OH detected within interstellar ices is not formed in the gas phase, but instead is formed by successive hydrogenation of CO accreted on the surface of dust grains.[107–109,111,112] The observation of higher CH_3OH abundances near massive protostars where ices are subjected to higher temperatures (30 K) and UV radiation, also suggests that it drives a rich interstellar photochemistry in these regions.[34,88] Hence understanding the adsorption and thermal desorption of CH_3OH ices provides an essential step towards elucidating the chemistry of interstellar and cometary ices.

4.2.1 Adsorption and desorption of pure CH_3OH ices on HOPG. Fig. 8 shows TPD spectra for pure CH_3OH ices adsorbed on HOPG at 98 K as a function of dose. At low exposures (Fig. 8A) two distinct peaks are observed in the TPD spectrum. The higher temperature peak is assigned to monolayer desorption. The low temperature peak that does not saturate with increasing dose (Fig. 8B) is assigned to the desorption of multilayer CH_3OH. Increasing the CH_3OH exposure further shows that multilayer desorption dominates the TPD spectrum. At the highest exposures (>100 L) (Fig. 8B) there is also a high temperature desorption peak, assigned to the formation of crystalline CH_3OH as a result of the heating process, as reaffirmed by RAIRS.[51] The formation of crystalline CH_3OH is dependent on the heating rate[177] as well as on the initial coverage and deposition temperature.[51]

Hydrogen bonding strongly influences the adsorption and desorption of CH_3OH on HOPG. Close inspection of the TPD data in Fig. 8B shows that the leading edges of the multilayer

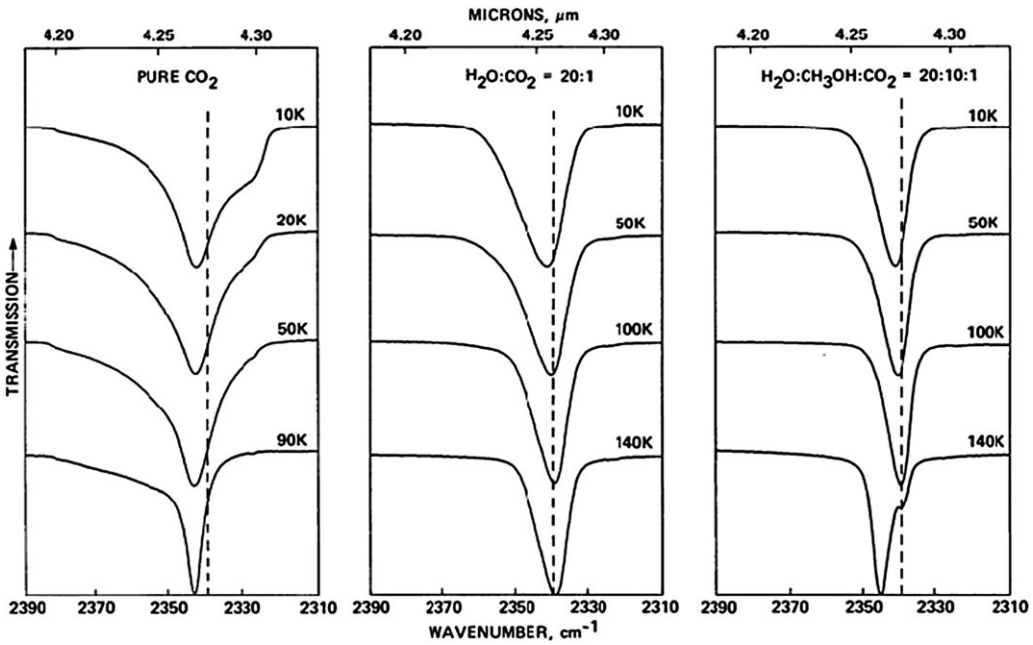

Fig. 7 The dependence of the $^{12}CO_2$ ν_3 band on temperature for three different matrix compositions. All the ices were deposited at 10 K and heated at a rate of 2 K min^{-1}. Annealing temperatures and ice compositions are shown in the figure. Reproduced from S. A. Sandford and L. J. Allamandola, *Astrophys. J.*, 1990, **355**, 357–372. Reproduced by permission of the AAS.

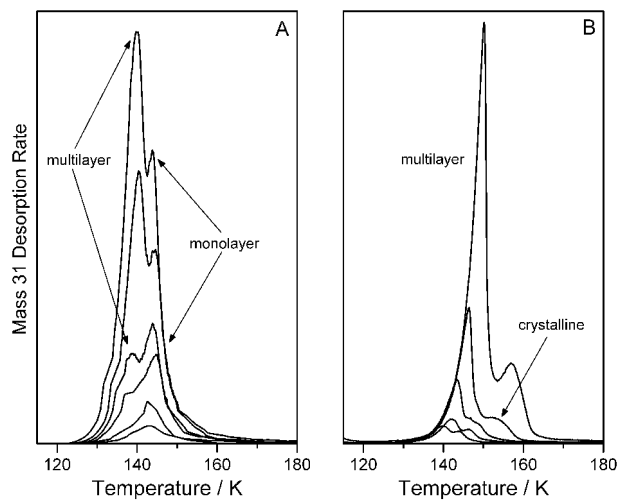

Fig. 8 TPD spectra for pure CH_3OH adsorbed on HOPG at 98 K following exposures of (A) 2, 3, 5, 7, 10 and 15 L and (B) 15, 20, 50, 100 and 300 L.

desorption peaks are not shared. Multilayer desorption typically obeys zero-order kinetics and is characterised by the sharing of the leading edges of TPD traces. The deviation from perfect zero-order desorption kinetics seen for CH_3OH (see Table 3) is ascribed to hydrogen bonding that exists within the ice. This is consistent with RAIRS data (not shown[51]), where hydrogen-bonded networks are evidenced by a characteristic broad ν(OH) stretching band. For adsorbates such as CH_3OH, where H-bonding is expected, the interactions between adjacent molecules, rather than adsorbate–substrate interactions, often dictate the adsorption. This is illustrated in Fig. 8, which clearly shows the onset of multilayer formation prior to monolayer saturation.

4.2.2 Sequentially deposited CH_3OH/H_2O ices. Pure CH_3OH ices are not found in interstellar conditions, and instead CH_3OH is usually found in H_2O-rich ices. It is therefore important to understand the interaction of CH_3OH with H_2O, in order to determine the complex chemistry of multi-component interstellar ices. The adsorption and desorption of CH_3OH ices from ASW films shows a complex interaction between the adsorbate and ASW, due to the formation of hydrogen bonds during thermal processing.[46] The strength of the interaction gives rise to changes in the RAIRS and TPD spectra of the underlying ASW ice film that are generally not observed for smaller, more volatile, species. When CH_3OH is deposited on the surface of ASW, perturbations in the resulting H_2O desorption are observed in the TPD spectra. The distinctive bump typically observed on the leading edge of the H_2O TPD trace,[137,195] ascribed to the ASW–CI phase transition, is not as prominent when compared with desorption of pure H_2O ice. RAIR spectra also suggest that crystallisation of the H_2O film may be modified in the presence of CH_3OH.

RAIRS data: adsorption and desorption of CH_3OH on ASW films. RAIR spectra recorded following the deposition of CH_3OH on top of ASW are almost identical to those for the pure ices grown on HOPG, implying that the ices form layers at 98 K.[46] Any differences between adsorption on bare HOPG and on ASW ices should be distinguishable only at the lowest adsorbate exposures, where the adsorbate is directly bound to the underlying substrate. However, RAIRS suggests that CH_3OH adsorption on ASW at low exposures is identical to adsorption on HOPG.[51] This is surprising, considering the presence of dangling OH bonds on the surface of ASW, which are expected to facilitate hydrogen bond formation.[147,148] However, it is possible that the ASW ice grown at 98 K is

Table 3 A summary of the experimentally derived kinetic parameters determined for the desorption of pure ices from HOPG at 97 K in our laboratory. The parameters were derived by leading edge analysis of TPD spectra. These parameters have been used to simulate the desorption of pure ices under astrophysical conditions

Molecule	Desorption order	Desorption energy/kJ mol^{-1}	Pre-exponential factor/molecules m^{-2} s^{-1}
Multilayer			
H_2O[52]	0.26 ± 0.02	39.9 ± 0.8	$1 \times 10^{27\pm1}$
CH_3OH[51]	0.35 ± 0.21	41.0 ± 0.8	$6 \times 10^{25\pm3}$
C_2H_5OH[57]	0.08 ± 0.07	56.3 ± 1.7	$2.2 \times 10^{37\pm2}$
NH_3[50]	0.25 ± 0.05	23.2 ± 1.1	$8 \pm 3 \times 10^{25}$
OCS[a]	0.11 ± 0.03	28.6 ± 1.3	$4.2 \times 10^{32\pm1}$
CO_2[a]	0	24.8 ± 162	$1.1 \pm 0.1 \times 10^{30}$
Monolayer			
CO_2[a]	0.73 ± 0.02	19.8 ± 2.9	$5.3 \pm 0.8 \times 10^{14}$ [b]
CH_3OH[51]	1.23 ± 0.14	48.0 ± 0.8	$9 \times 10^{9\pm3}$ [b]

[a] The substrate temperature in these experiments was $\leq$20 K. [b] Monolayer desorption is first order and therefore the pre-exponential factor has units of s^{-1}.

not sufficiently porous to modify adsorption of the CH_3OH monolayer compared to on HOPG.

To investigate the thermal processing and desorption of the ices, annealing experiments were performed using RAIRS. RAIRS complements TPD data (shown later) by probing the structural changes of the ices during annealing and identifying any molecular interactions that occur between the ices. Fig. 9 compares RAIR spectra following the annealing of 50 L of CH_3OH ice on HOPG and 50 L of CH_3OH deposited onto a 50 L ASW film grown on HOPG. The changes to the OH and CO band profiles during the annealing of CH_3OH on ASW are in contrast to those observed for pure CH_3OH on HOPG. Furthermore, the changes to the OH stretch shown in Fig. 9C are different to those observed for pure H_2O ices.[52] Annealing the pure CH_3OH ice to 129 K results in the splitting of both the OH and CO bands, prior to desorption from the HOPG surface at 160 K. The OH band splits into two peaks at 3290 cm^{-1} and 3174 cm^{-1} (Fig. 9D). Similarly the CO band splits at 129 K into peaks at 1037 cm^{-1} and 1027 cm^{-1} (Fig. 9B). In each case, these observations were assigned to a change in morphology of the CH_3OH ice from an amorphous to a crystalline phase, prior to desorption.[51]

It is evident from the RAIRS data shown in Fig. 9A and C that annealing the binary ices does not lead to the crystallisation of the CH_3OH overlayer. The CO band (Fig. 9A) does not split into two peaks during annealing, but instead heating to 135 K results in a decrease in the intensity of the CO stretch at 1045 cm^{-1}, coupled with a downshift in frequency to 1038 cm^{-1} and the appearance of a low frequency shoulder at 1013 cm^{-1}. The 1013 cm^{-1} feature is not observed in the pure CH_3OH ice (Fig. 9B), suggesting that an interaction occurs between the CH_3OH and H_2O ice layers on heating. It will be shown later from TPD data and from studying CH_3OH : H_2O mixed ices that this new band arises from thermally induced mixing between the ices. Intermixing between the ices during annealing is further supported by the fact that the CO band remains in the RAIR spectrum to higher temperatures when deposited on ASW (Fig. 9A) compared to on HOPG (Fig. 9B), consistent with experiments performed on CH_3OH and D_2O layered ices.[196,197]

TPD data. TPD data for CH_3OH deposited on ASW films provide further evidence that ASW significantly changes the desorption of volatiles deposited on its surface. TPD spectra

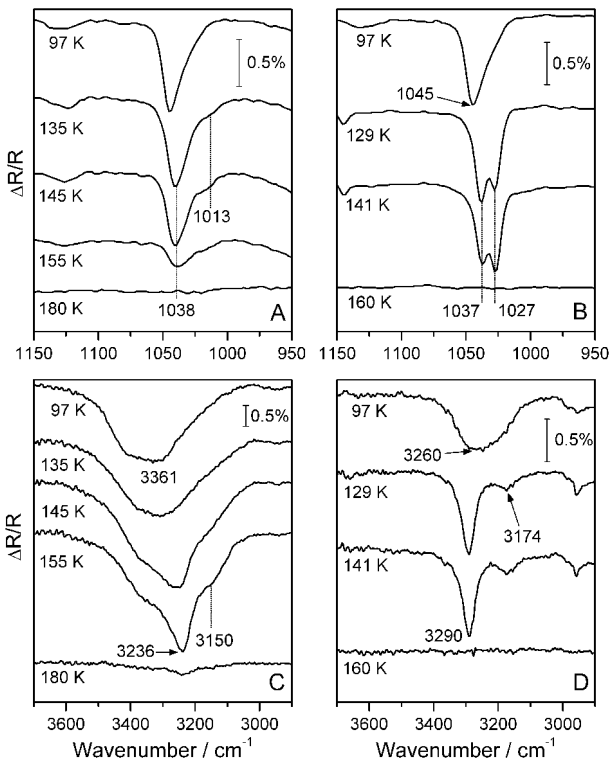

Fig. 9 RAIR spectra comparing the sequential heating of 50 L CH_3OH deposited on 50 L H_2O (A and C) with 50 L of pure CH_3OH ice (B and D). (A) and (B) show the CO stretching region between 1150 and 950 cm^{-1}. (C) and (D) focus on the OH stretching region between 3700 and 2900 cm^{-1}. In each case the underlying substrate was HOPG and the deposition temperature was 97 K. The annealing temperatures are shown in the figure.

following increasing exposures of CH_3OH adsorbed on 50 L of ASW on HOPG at 97 K are shown in Fig. 10. It is immediately clear when comparing TPD spectra for CH_3OH adsorbed on ASW with those for CH_3OH deposited directly onto HOPG (Fig. 8) that very different behaviour is observed. In contrast to the two well defined monolayer and multilayer peaks observed when CH_3OH is deposited on HOPG, CH_3OH desorption from ASW is complex. Assignment of the desorption peaks in Fig. 10 was made by comparison with TPD spectra for CH_3OH desorption from HOPG (Fig. 8) and by

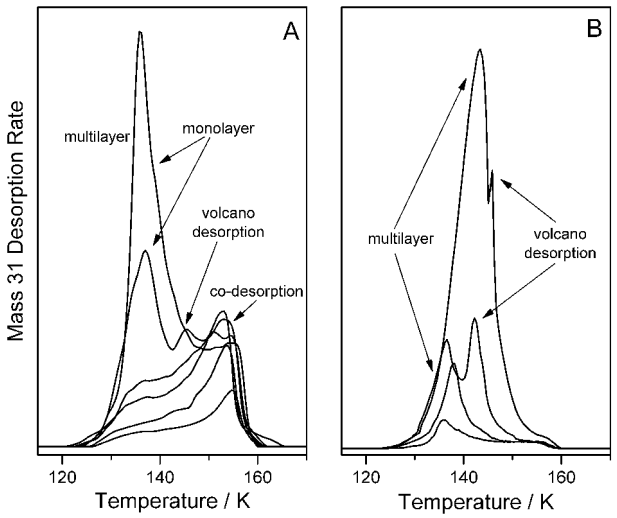

Fig. 10 TPD spectra following increasing CH_3OH exposures on a 50 L ASW film adsorbed on HOPG at 97 K. (A) shows CH_3OH exposures of 3, 5, 7, 10, 15 and 20 L. (B) shows CH_3OH exposures of 20, 50, 100 and 300 L.

correlating CH_3OH desorption with the corresponding H_2O TPD spectrum.[52]

Fig. 11A compares TPD spectra of pure CH_3OH ice adsorbed on HOPG with CH_3OH adsorbed on 50 L ASW on HOPG at 97 K. The figure clearly shows that the monolayer peak for the pure CH_3OH ice desorbs at a similar temperature to the peak observed around 137 K for CH_3OH adsorbed on ASW. Hence this peak can be assigned to a CH_3OH monolayer desorbing from the ASW surface. However, the desorption of the CH_3OH monolayer is clearly modified on ASW. The broadening of the monolayer TPD profile, and the relative decrease in the intensity of the monolayer peak on the ASW surface, is consistent with the heterogeneity of the porous ASW film.[127,145,146,182]

The CH_3OH multilayer can be assigned based on the observation of similar behaviour for CH_3OH adsorbed on HOPG and on ASW (Fig. 11B). This peak does not saturate and is characterised by an increase in desorption temperature with increasing dose, in addition to an asymmetric peak profile. The presence of both monolayer and multilayer features is consistent with previously reported CH_3OH/H_2O data.[67] The desorption kinetics of the multilayer are clearly modified when adsorbed on ASW. A similar modification of adsorbate desorption kinetics has also been observed for C_2H_5OH/H_2O ices[69] and D_2 desorption from ASW surfaces.[146,182] This is shown in Fig. 11B, which compares the TPD traces of multilayer CH_3OH (300 L) adsorbed on H_2O ice of varying thickness (10 L and 50 L) and on bare HOPG. The H_2O exposures correspond to a non-porous monolayer H_2O film (10 L) and a porous ASW ice layer (50 L). A detailed discussion of the effect that these H_2O films have on the thermal desorption of CH_3OH can be found in Wolff *et al.*[46] For the purposes of this discussion, the films reflect a change in surface morphology, ranging from bare HOPG to ASW. The change in kinetics is characterised by an increase in desorption temperature and by the fact that the leading edges of multilayer traces on the different surfaces cannot be overlaid.

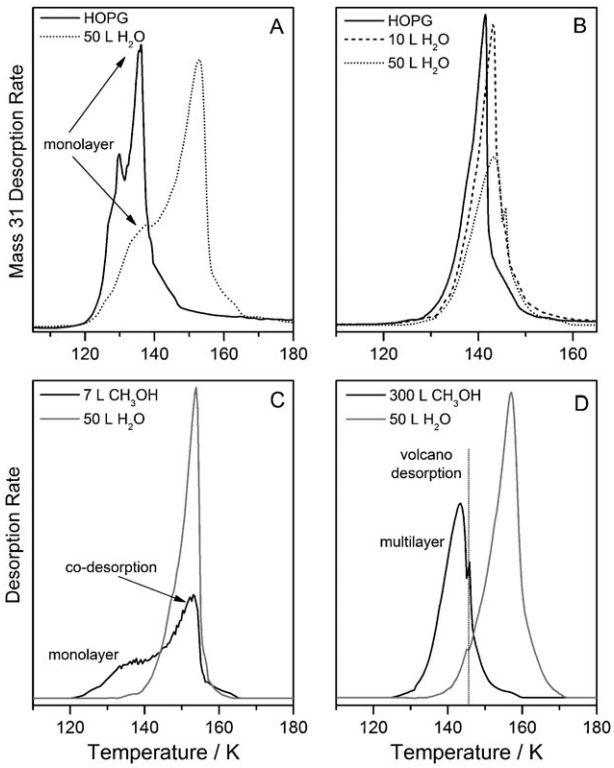

Fig. 11 (A) TPD spectra comparing the desorption of 7 L of CH_3OH deposited on bare HOPG (solid line) with 7 L CH_3OH deposited on 50 L H_2O (dotted line). (B) Comparison of CH_3OH TPD spectra adsorbed on bare HOPG (solid line) and H_2O films of 10 L (dashed line) and 50 L (dotted line). The CH_3OH exposures in (B) were 300 L in each case. Panels C and D show TPD spectra overlaying CH_3OH desorption traces (black lines) with the corresponding H_2O desorption traces (grey lines) for layered ices. The CH_3OH exposures are 7 L (C) and 300 L (D). The H_2O TPD spectrum in (A) has been scaled for clarity. In all cases the deposition temperature was 97 K.

Adsorption of CH_3OH on ASW (Fig. 10) also gives rise to two additional desorption features that are not observed in the pure ices (Fig. 8). Assignment of the new features can be made by overlapping the respective CH_3OH and H_2O TPD spectra obtained from a single experiment. At low CH_3OH exposures (7 L), Fig. 11C shows that the high temperature feature (154 K) observed in the CH_3OH TPD corresponds to the desorption of bulk crystalline H_2O ice. This peak can therefore be assigned to CH_3OH co-desorption with CI. At higher CH_3OH exposures (300 L), Fig. 11D shows that the sharp feature observed on the high temperature side of the CH_3OH multilayer corresponds to the ASW–CI phase transition in the underlying ASW ice (146 K), and can therefore be assigned to CH_3OH desorption *via* a volcano desorption mechanism. Volcano and co-desorption of CH_3OH have also been reported in other TPD experiments investigating CH_3OH desorption from ASW.[67]

The presence of both co-desorption and volcano features indicates that thermally induced mixing occurs between the two ice layers. However, the extent of the mixing is difficult to fully assess with TPD and RAIRS alone. As shown in Fig. 10, monolayer CH_3OH desorbs from the ASW surface prior to the saturation of the co-desorption feature, suggesting that not all

of the CH_3OH is incorporated into the H_2O ice even at low CH_3OH exposures. Thermally induced mixing for the layered ices has been ascribed to the entrapment of CH_3OH at grain boundaries during the ASW–CI transition,[46] rather than a complete mixing between the two films as previously reported in experiments on CH_3OH/D_2O ices[196,197] and C_2H_5OH/H_2O layered ices.[69,198]

4.2.3 CH_3OH : H_2O ice mixtures

TPD data. The most astronomically relevant ices consist of intimate mixtures of the various components of the ice. Fig. 12A shows TPD spectra recorded for CH_3OH and H_2O following a 300 L exposure of a mixed CH_3OH : H_2O ice on HOPG at 97 K. The TPD spectrum for H_2O resembles that observed for pure H_2O ices adsorbed on HOPG.[52] The main peak at 166 K is assigned to the desorption of CI, and the high temperature shoulder at 172 K is assigned to the desorption of hexagonal ice. However, there are also some subtle changes to the H_2O TPD profile due to the presence of CH_3OH within the ice. Firstly, the bump on the leading edge of the H_2O TPD spectrum, characteristic of the ASW–CI phase transition,[137,195] is not observed for mixed CH_3OH : H_2O ices. This is consistent with previous studies of layered CH_3OH/H_2O ices which showed that CH_3OH lowers the crystallisation temperature of H_2O ice when incorporated into the underlying bulk, by inducing the nucleation of H_2O.[186] Secondly, the feature assigned to hexagonal ice is more prominent compared to that seen for the pure H_2O ice[52] and that observed for the binary layered ices.[46] This is ascribed to a strong interaction between CH_3OH and H_2O and will be discussed later.

CH_3OH desorption from the ice mixture is characterised by three main features. The TPD spectrum is dominated by a broad desorption peak with an onset around 133 K, and a local maximum at 144 K. This is followed by a complex irregular desorption profile. This complex multi-component feature is contrasted by a well defined sharp desorption peak at 166 K, coupled with a broad low intensity shoulder appearing on the high temperature side of this peak at 172 K. It is clear from the TPD data (Fig. 12A) that CH_3OH desorption from the mixed ice is significantly modified compared to the desorption of pure CH_3OH ice and CH_3OH/H_2O layered ices. This is shown in Fig. 12B which compares the TPD trace for CH_3OH from the mixed ices (Fig. 12A) with TPD traces for equivalent exposures of pure CH_3OH (black line panel B) and CH_3OH deposited on 50 L of ASW at 97 K (grey line panel B).

Fig. 12A shows that the two CH_3OH peaks at 166 and 172 K desorb coincidentally with the crystalline and hexagonal phases of H_2O respectively. These features are therefore assigned to the co-desorption of CH_3OH trapped within the bulk of the H_2O ice. The fact that the CH_3OH also desorbs with hexagonal ice implies a strong interaction between CH_3OH and H_2O. RAIRS data (not shown) suggest that this interaction is due to the formation of a hydrogen-bonded complex.

The complexity of the broad low temperature feature in Fig. 12A suggests desorption from numerous sources. Clearly, CH_3OH desorption occurs prior to the onset of H_2O desorption at 133 K. Hence this feature is not a result of CH_3OH desorption *via* a molecular volcano mechanism. Furthermore, this feature is very broad compared to the sharp

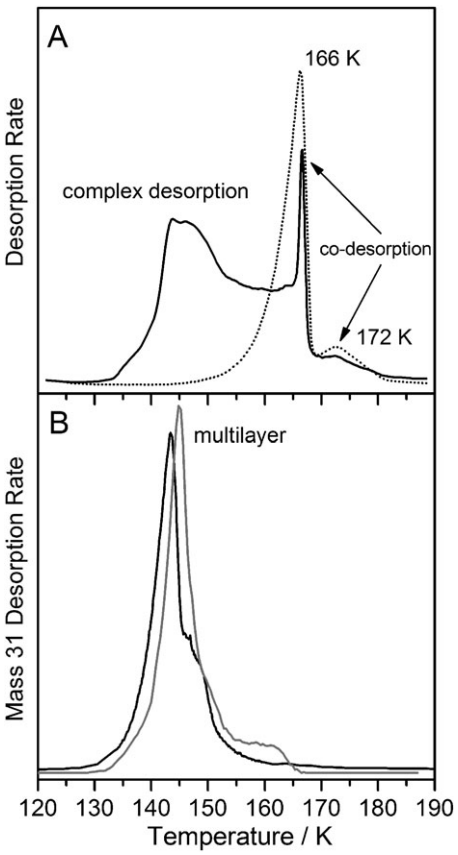

Fig. 12 (A) TPD spectra overlaying desorption traces of CH_3OH (solid line) and H_2O (dotted line) following an exposure of 300 L of a mixed ice adsorbed on HOPG at 97 K. The composition of the ice was 16% CH_3OH. The H_2O TPD trace has been scaled for clarity. (B) TPD spectra for pure CH_3OH ice adsorbed on HOPG at 97 K (black line) and CH_3OH deposited on a 50 L exposure of ASW at 97 K (grey line). In each case the CH_3OH exposure was 50 L, corresponding to an equivalent dose of CH_3OH as in the mixed ice.

and well defined desorption typically characteristic of explosive volcano desorption as observed for OCS (see later) and other volatile species.[48,65–67,137] Fig. 12B shows that the broad CH_3OH feature observed in the mixtures has a desorption temperature corresponding to CH_3OH desorption from both HOPG and ASW films. This suggests that CH_3OH desorption from the mixture still occurs near its natural sublimation temperature on HOPG or ASW and is not completely inhibited when co-deposited. This could imply that CH_3OH has the ability to diffuse through the ASW ice. However, the complex CH_3OH feature could also be a result of the phase change of the ASW. Previous experiments[135,136,196,199] have shown that ASW undergoes a morphology change at 136 K, exhibiting liquid-like properties prior to crystallisation at 165 K. This is consistent with desorption of CH_3OH across this temperature range. Whether CH_3OH has the ability to diffuse through the ice in a similar fashion to smaller volatiles (CO_2, CO), or whether desorption is induced by the rearrangement of the ASW prior to crystallisation, cannot be determined here. However, the TPD data clearly indicate the presence of two distinct CH_3OH species within the H_2O ice. One species gives rise to co-desorption in the TPD spectrum. The second species

is more weakly bound within the ASW ice and desorbs prior to crystallisation, most likely during the phase transition of liquid-like water.

RAIRS data: adsorption and desorption of mixed CH_3OH : H_2O ices on HOPG. Fig. 13 shows a RAIR spectrum following a 300 L exposure of a CH_3OH : H_2O mixture on HOPG at 97 K. Assignment of the vibrational bands is straightforward, based on comparison with RAIR spectra obtained for pure H_2O[52] and pure CH_3OH[51] ices adsorbed on HOPG. The dominant band in the RAIR spectrum occurs between 3600 cm^{-1} and 3000 cm^{-1} and is assigned to the ν(OH) stretch of H_2O. The low intensity broad bands at 2247 cm^{-1} and 1677 cm^{-1} are assigned to the lateral OH bending mode and the HOH scissors mode of H_2O respectively. The broad intense feature centred at 881 cm^{-1} is a frustrated libration mode of H_2O.[200] The remaining infrared bands can be confidently assigned to vibrational modes arising from the CH_3OH within the ice. However, some infrared bands observed for pure CH_3OH are not observed in the mixture. The ν(OH) band at 3260 cm^{-1}, assigned to CH_3OH in the pure RAIRS spectrum,[51] is obscured by the ν(OH) band of H_2O, which also masks the CH_3OH $\nu_a(CH_3)$ stretch. The slight broadening and downshift of the H_2O ν(OH) band in the mixtures compared to that of the pure H_2O ice[52] is indicative of hydrogen bonding between H_2O and CH_3OH, as expected, as also observed for sequentially deposited CH_3OH/H_2O ices.[46,196,197]

The most significant difference between the pure CH_3OH spectrum and the CH_3OH : H_2O spectrum is the splitting of the CH_3OH ν(CO) band, shown in the inset to Fig. 13. When CH_3OH is adsorbed on HOPG, the ν(CO) band gives a single peak located at 1045 cm^{-1}. There is no change to either the band profile or position when CH_3OH is adsorbed on a 50 L thick ASW film (Fig. 9).[46] However when CH_3OH is co-deposited with H_2O, the band is downshifted and split into two distinct peaks at 1035 and 1018 cm^{-1} (Fig. 13 inset). The splitting of the ν(CO) band suggests that CH_3OH resides in two distinct environments within the ice. Recent experiments in our laboratory have shown that this is probably a thermal effect, since deposition of identical CH_3OH : H_2O ice mixtures at temperatures <14 K gives rise to a single ν(CO) peak at 1028 cm^{-1}. Heating these ices to $\sim$90 K results in the splitting of the ν(CO) band into two peaks at 1035 and 1018 cm^{-1}, as seen in Fig. 13.

The desorption of the ice mixtures was investigated by performing a series of annealing experiments. Fig. 14 shows RAIR spectra resulting from annealing 300 L of an 11% CH_3OH : H_2O ice adsorbed on HOPG at 97 K. The changes observed in the ν(OH) band of the CH_3OH : H_2O ices during annealing are almost identical to those reported for pure H_2O adsorbed on HOPG.[52] The sharpening of the ν(OH) band, in addition to the change in relative intensities of the two shoulders at 145 K, is characteristic of ASW crystallisation.[52,201] Comparing the ν(OH) band of the CH_3OH : H_2O mixtures with that of CH_3OH/H_2O binary layers (Fig. 9C) during annealing shows distinct differences between the two systems. Furthermore the ν(OH) band remains in the RAIR spectrum to higher temperatures for the mixtures. The difference in the ν(OH) band profile between the mixtures (Fig. 14A) and the binary layers (Fig. 9C) is a direct result of the concentration of CH_3OH in the ice. Experiments performed with ice mixtures with a 60% concentration of CH_3OH (not shown) show similar changes in the ν(OH) band profile compared to those observed for the binary layers.

Fig. 14B shows the effect of annealing 300 L of the CH_3OH : H_2O ice, focusing on the ν(CO) infrared bands

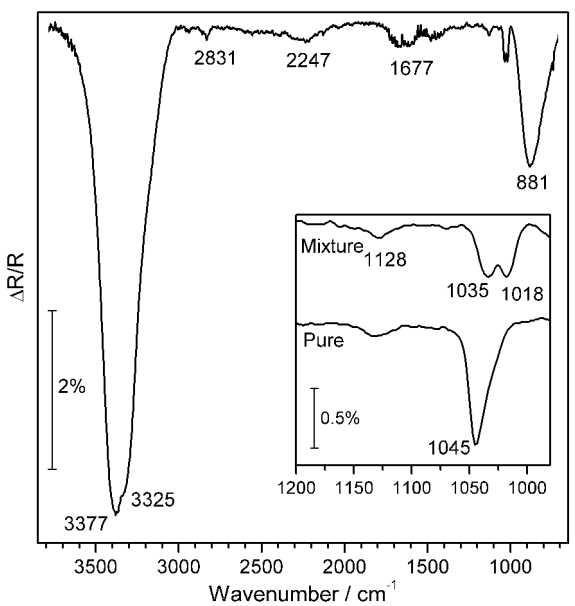

Fig. 13 RAIR spectra following a 300 L exposure of a CH_3OH : H_2O mixture on HOPG at 97 K. The composition of the mixture (in the vapour phase) was approximately 11% CH_3OH. The inset shows the spectrum between 1200 and 950 cm^{-1} in more detail and also includes a RAIR spectrum of a 50 L exposure of pure CH_3OH ice adsorbed on HOPG at 97 K.

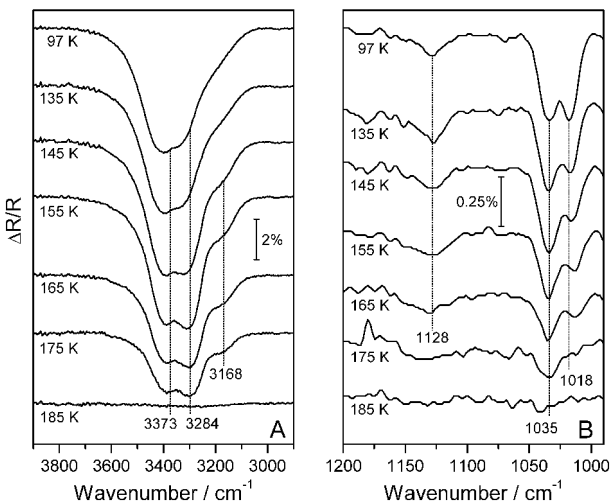

Fig. 14 RAIR spectra showing the effects of sequential annealing of a 300 L exposure of an 11% CH_3OH : H_2O ice adsorbed on HOPG. (A) shows the high frequency region between 3900 and 2900 cm^{-1}, highlighting the crystallisation of ASW to CI. (B) shows the low frequency region between 1200 and 990 cm^{-1}, showing the effects of annealing the ice on the ν(CO) band of CH_3OH. The annealing temperatures are shown in the figure.

between 1200 cm^{-1} and 990 cm^{-1}. The 1018 cm^{-1} band shows an immediate decrease of intensity at an annealing temperature of 135 K. A continued decrease in intensity of this peak is observed until desorption is complete at 175 K. In contrast, the band at 1035 cm^{-1} shows no change in peak intensity until an annealing temperature of 155 K, and remains in the spectrum to a slightly higher temperature of 185 K. The remaining features in the RAIR spectrum, assigned to CH_3OH, also show a gradual decrease of intensity, until desorption is complete by 175 K. The contrasting behaviour of the two ν(CO) bands during the annealing of the CH_3OH : H_2O ice confirms the fact that CH_3OH resides in two different environments in the mixed ice. This is further evidenced by comparing the behaviour of the split ν(CO) band with the TPD data shown in Fig. 12. The 1035 cm^{-1} ν(CO) band can be correlated with the high temperature co-desorption features observed in the TPD. The complex feature in the TPD spectrum is associated with the 1018 cm^{-1} ν(CO) vibrational band in the RAIRS. This band begins to desorb at an annealing temperature of 135 K, consistent with observations in the TPD.

Bringing the data from the RAIRS and TPD together shows that H_2O significantly modifies the thermal desorption behaviour of CH_3OH when compared to desorption from the pure ices. CH_3OH desorption from the ices is dependent on the exact interaction with H_2O. Weak CH_3OH : H_2O interactions give rise to a complex peak in the TPD, observed at temperatures corresponding to the sublimation temperature of pure CH_3OH and to the ASW to CI phase transformation. Strong CH_3OH : H_2O interactions give rise to co-desorption features with CI and hexagonal ice.

The formation of a clathrate-hydrate has previously been proposed to explain the interaction of CH_3OH with H_2O within mixed CH_3OH : H_2O ices.[64,157,187,191] Furthermore, the presence of clathrate hydrates has also been suggested to account for the release of trapped gases from cometary ices when the ice is warmed at large distances from the sun. Blake *et al.* demonstrated that CH_3OH forms type II clathrate hydrates at 130 K, following deposition of a H_2O : CH_3OH (20 : 1) mixture at 85 K.[187] Experiments performed at higher CH_3OH concentrations gave rise to phase separation, with the formation of a type II clathrate-hydrate in addition to regions of pure amorphous CH_3OH that were segregated at grain boundaries. Similar experiments by Hudson and Moore also confirmed the formation of a CH_3OH clathrate in CH_3OH : H_2O ices using infrared spectroscopy.[191] Hence, the formation of a clathrate-hydrate structure, in addition to thermally induced CH_3OH segregation, could explain the splitting of the ν(CO) band observed in the CH_3OH : H_2O RAIRS shown in Fig. 14.

4.3 Adsorption and desorption of model OCS interstellar ices

OCS has been detected in several astrophysical environments including planetary atmospheres within our own solar system,[202] cometary comae[203] and within icy mantles in dense molecular clouds.[75,204–206] However, compared to CH_3OH, OCS has received considerably less attention in the astrophysical literature, mainly because it is detected in much smaller abundances, estimated to be 0.05–0.2% with respect to H_2O.[75,204–206] Detection of solid OCS within interstellar ices has been confirmed by a combination of theoretical and laboratory infrared studies of multi-component OCS ices at 10 K.[205,206] The 4.9 μm (2040 cm^{-1}) absorption feature observed within astrophysical spectra was attributed to the CO stretch of OCS. This infrared band was shown to be highly sensitive to the ice environment,[207] with OCS thought to be embedded within CH_3OH-rich ices.[205,206] Astrophysical models of sulfur chemistry in hot core regions have successfully predicted the observed gas phase abundances of the majority of sulfur containing species, including SO, SO_2 and CS.[208,209] However, OCS abundances cannot be reproduced *via* gas phase reactions, hence surface chemistry is implied.[208,209] As a result laboratory studies have shown that OCS can be readily produced *via* UV[210] and proton irradiation[211] of ices including carbon (CO and CO_2) and sulfur (H_2S and SO_2) containing species. Despite the obvious importance of OCS, its thermal desorption from dust grain analogues has not previously been reported in detail.

4.3.1 Adsorption and desorption of pure OCS ices adsorbed on HOPG. TPD and RAIRS data show that OCS is weakly bound to the HOPG surface at 14 K, forming physisorbed multilayer ices. This is confirmed by the relatively low desorption energy determined for the multilayer species from leading edge TPD analysis (see later) and the fact that the infrared bands in the RAIR spectra remain unsaturated as a function of increasing ice exposure (not shown).

OCS monolayer and multilayer features can be distinguished at low exposures (<5 L) by the presence of two distinct TPD peaks. For increased exposures between 7 and 10 L these peaks merge into a single desorption feature. TPD traces for multilayer OCS desorption from HOPG (Fig. 15 trace A) are in good agreement with previously published data for OCS desorption from Au.[67] In contrast to CH_3OH ices, OCS shows no evidence of clustering on HOPG at low exposures.

The most significant information that can be obtained from TPD investigations of pure ices is the determination of the kinetic parameters for desorption. Desorption orders, energies and pre-exponential factors can be determined from a series of TPD spectra such as those shown in Fig. 8. These can then be incorporated into astronomical models to simulate desorption on astronomically relevant time scales.[55]

There are a variety of analytical methods that can be used to determine kinetic information from a series of thermal desorption curves with varying initial exposures.[180,181] The method described here has been successfully used to determine desorption parameters for all six adsorbates investigated in our laboratory to date, and the kinetic parameters obtained are summarised in Table 3. Specifically, data have been obtained for the desorption of multilayer H_2O,[52] CH_3OH,[51] NH_3[50] and C_2H_5OH[57] adsorbed on HOPG at 97 K and for the desorption of multilayer CO_2 and OCS ices adsorbed on HOPG at 14 K. Values for the desorption of monolayer CO_2 and CH_3OH[51] are also reported. Here we discuss the analysis of TPD data for pure OCS ices, to obtain the desorption parameters given in Table 3.

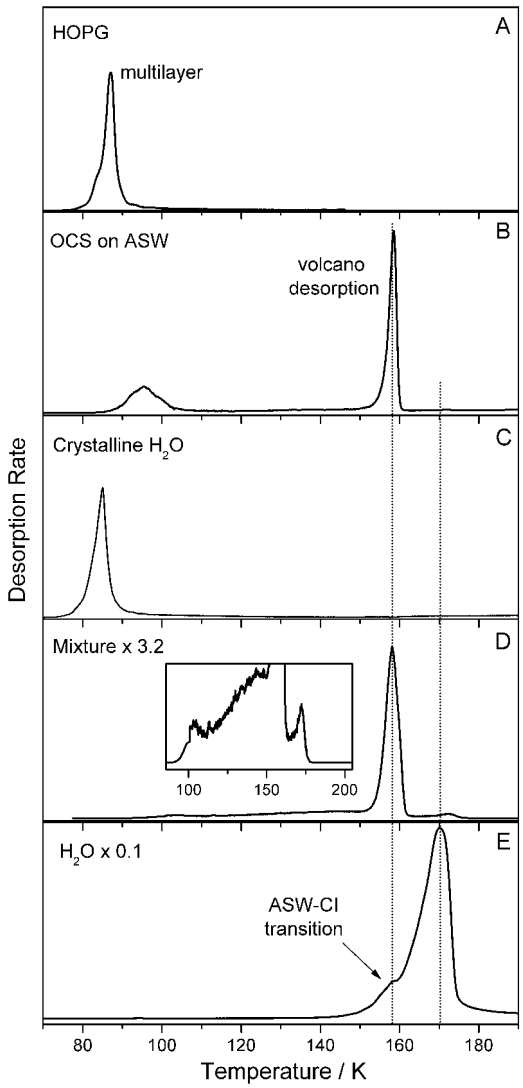

Fig. 15 TPD spectra showing 15 L OCS desorption from (A) bare HOPG, (B) 100 L of ASW ice grown on HOPG, and (C) crystalline H_2O formed by annealing ASW to 150 K for 3 minutes. (D) shows OCS desorption from a 100 L exposure of mixed ice with a composition of 8% OCS with respect to H_2O. A scaled H_2O spectrum (E) is also shown for comparison. In each case the deposition temperature was 14 K.

Desorption orders. The starting point of any TPD analysis is the Polanyi–Wigner equation:[180,181]

$$r_{\mathrm{des}} = -\frac{\mathrm{d}\theta}{\mathrm{d}t} = \upsilon_n \theta^n \exp\left(\frac{-E_{\mathrm{des}}}{RT}\right) \qquad (1)$$

where r_{des} is the rate of desorption, θ the adsorbate coverage, υ_n is the desorption pre-exponential factor, n is the order of desorption, E_{des} is the desorption activation energy, R is the gas constant, T the substrate temperature and t is time. Since the rate of change of coverage θ with time t can be linked, *via* a linear heating rate, to the rate of change of coverage θ with temperature T (which is proportional to the signal intensity in the TPD trace $I(T)$), eqn (1) becomes:

$$I(T) \propto \upsilon_n \theta^n \exp\left(\frac{-E_{\mathrm{des}}}{RT}\right) \qquad (2)$$

Rearranging this equation and taking logarithms, and noting that only relative coverage θ_{rel} can be measured in the experiments described here, eqn (2) becomes:

$$\ln[I(T)] \propto \ln(\upsilon_n) + n\ln(\theta_{\mathrm{rel}}) - \frac{E_{\mathrm{des}}}{RT} \qquad (3)$$

The desorption order can then be obtained by plotting a graph of $\ln[I(T)]$ against $\ln[\theta_{\mathrm{rel}}]$ for a series of TPD curves of varying initial coverage at a fixed temperature. The gradient of this plot is equal to the desorption order n. In order to successfully perform this plot, the values of E_{des} and υ_n should not vary significantly with coverage. This plot is constructed from points taken from the leading edges of the TPD curves at a fixed temperature. Average desorption orders can be obtained by repeating the plot for a range of fixed temperatures. This calculation is ideally performed for a family of TPD curves consisting of a single desorption peak.

However, weakly bound states often give rise to monolayer and multilayer species, characterised by a significant degree of overlap between the desorbing species. This is observed for OCS, shown in Fig. 16A. As a result, order plots are constructed using a range of temperatures that incorporate contributions from all desorption peaks. Despite this difficulty, the methodology has been shown to successfully generate reproducible desorption orders that are consistent with conclusions that may be drawn from direct observation of the TPD data. An example for OCS is shown in Fig. 16B, which shows a plot of $\ln[I(T)]$ against $\ln[\theta_{\mathrm{rel}}]$ at a fixed temperature of 84 K. The dotted line in Fig. 16A indicates the points on the TPD traces from which the order plot was constructed. The plot exhibits two clear gradients over the exposure range. This can be explained by reference to the TPD data in Fig. 16A and with regard to the temperature used to construct the plot. The gradient of the plot corresponds to the most dominant peak in the TPD spectrum at the selected temperature. Hence points obtained for exposures ≤ 10 L pass through the leading edge of the monolayer peak, giving rise to a slope corresponding to the order of desorption for the monolayer ($n = 1.64 \pm 0.03$). Similarly, points for exposures > 10 L are dominated by contributions from the multilayer, and yield a slope giving the desorption order for the multilayer ($n = 0.11 \pm 0.03$).

Desorption for multilayer ices is expected to follow zero-order kinetics, and this is often assumed in TPD analysis of astrophysically relevant ices.[44,45,48,49,97,177] However it is clear from the desorption orders shown here (Table 3) that multilayer ices do not always show perfect zero-order desorption kinetics. It will be shown later that the accurate determination of the desorption order is an important factor, not only in the determination of the subsequent kinetic parameters such as E_{des} and υ_n that are derived from its value, but also in relation to modelling desorption under astrophysical conditions.

Desorption energy. Using the calculated desorption orders, the energy of desorption can be obtained by further rearrangement of eqn (3):

$$\ln[I(T)] - n\ln\theta_{\mathrm{rel}} \propto \ln\upsilon_n - \frac{E_{\mathrm{des}}}{RT} \qquad (4)$$

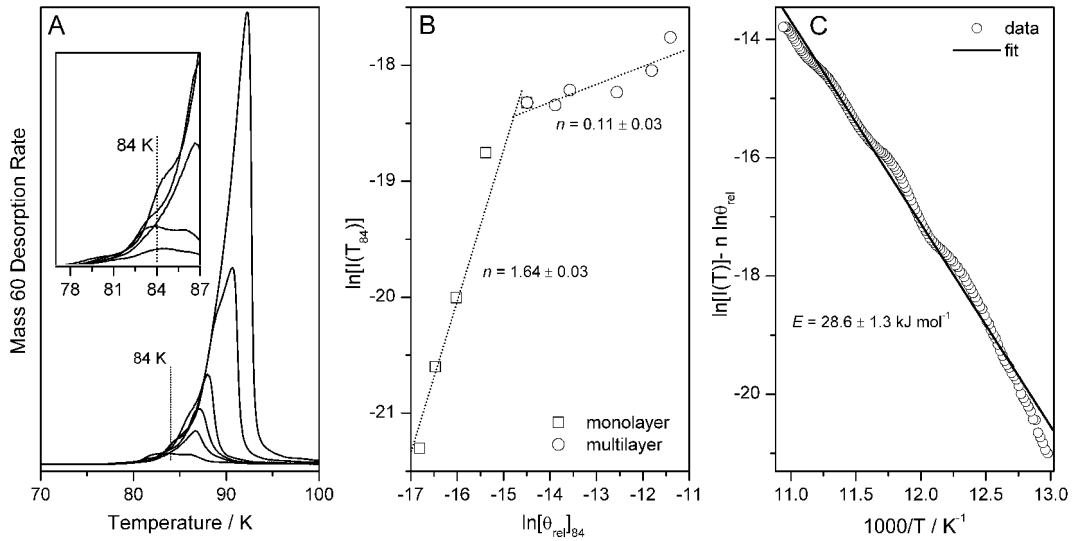

Fig. 16 Plots showing how the desorption order, n and desorption energy, E_{des} are obtained for the series of OCS TPD curves shown in (A). (B) shows a graph of $\ln[I(T)]$ against $\ln(\theta_{rel})$ at a fixed temperature of 84 K and allows the determination of the order of desorption. (C) shows a graph of $\ln[I(T)] - n\ln(\theta_{rel})$ against $1/T$ for multilayer OCS following an exposure of 100 L of OCS on HOPG at 14 K. The data are plotted with a desorption order of $n = 0.11$. The desorption energy is calculated from the gradient $-E_{des}/R$.

Hence plotting $\ln[I(T)] - n\ln(\theta_{rel})$ against $1/T$ for the leading edge of a single TPD spectrum (*i.e.* for a single exposure), yields a plot with a straight line of gradient $-E_{des}/R$ for the correct order of desorption. Fig. 16C shows a typical plot of $\ln[I(T)] - n\ln(\theta_{rel})$ against $1/T$ for a 100 L exposure of OCS on HOPG, giving a desorption energy of 28.6 ± 1.3 kJ mol^{-1} for multilayer OCS.

Pre-exponential factors. The pre-exponential factors for molecular ice desorption from HOPG are calculated using the values of desorption order (n) and desorption energy (E_{des}) obtained from the TPD experiments. The pre-exponential factor is usually obtained from an Arrhenius plot where the absolute coverage of the ice is known. However, in our experiments the absolute coverage is not known. Hence a simple method has been developed to estimate the pre-exponential factor (υ_n) using the following expression:

$$\upsilon_n = \frac{I_s(T)}{\theta_s^n \exp\left[\frac{-E_{des}}{RT}\right]} \qquad (5)$$

Here $I_s(T)$ is the scaled mass spectrometer intensity and θ_s is the scaled coverage determined from $I_s(T)$. The scaled values for $I_s(T)$ and θ_s used in eqn (5) are calculated from a scaling factor that directly relates the number of molecules per unit area adsorbed on the HOPG surface to a saturated monolayer coverage observed in the TPD spectra. The latter is determined by estimating the surface area for monolayer saturation from the area and density of the ice, and correlating this to the integrated area under the monolayer peak in the TPD spectrum. This value is then used to convert the experimentally measured relative intensities and coverages into absolute values. The value determined for the pre-exponential factor for OCS multilayer ice is given in Table 3. A more detailed description of this analysis method can be found elsewhere.[50,52,57]

4.3.2 Sequentially deposited OCS/H_2O ices

RAIRS: adsorption and desorption of OCS on ASW films. As for CH_3OH, understanding the interaction of OCS with H_2O ice is also important to help elucidate the behaviour of real interstellar ices. The RAIR spectra of OCS deposited on ASW can only be distinguished from OCS adsorption on HOPG at the lowest exposures (submonolayer coverages), where surface interactions are dominant. The CO band of OCS on ASW exhibits a downshift of ~ 12 cm^{-1} compared to adsorption on HOPG. Increasing the OCS exposure leads to the formation of multilayers, yielding infrared spectra that are identical to those observed for multilayer OCS adsorbed on HOPG (not shown).

RAIR spectra showing the changes to the OCS CO vibrational band during the annealing of 100 L OCS deposited on 100 L ASW (Fig. 17B) clearly show that its thermal behaviour is significantly modified compared to pure OCS ice adsorbed directly on HOPG (Fig. 17A). The complex changes observed in the OCS CO band on HOPG during annealing (Fig. 17A) are assigned to a phase change prior to desorption at 80 K.[207] However these changes are clearly not observed for the OCS/H_2O ice system. Analogous to the annealing behaviour of CH_3OH on ASW, the phase change of the OCS is inhibited by the underlying ASW ice. However the thermal desorption behaviour of ASW itself remains unchanged in the OCS/ASW ices. Furthermore, OCS is also retained on the ASW surface to much higher temperatures (145 K) compared to identical exposures grown on bare HOPG (80 K) providing clear evidence that OCS remains trapped within ASW.

TPD data. In contrast to the complex desorption exhibited in the CH_3OH/ASW ice system, the OCS/ASW layered ices provide a much clearer example of how ASW traps astrophysically relevant volatiles as shown in Fig. 15. Comparing the TPD profile of multilayer OCS desorption (15 L) around 90 K from HOPG (trace A) with that of OCS desorption from ASW (trace B), there is a clear broadening and reduction in the

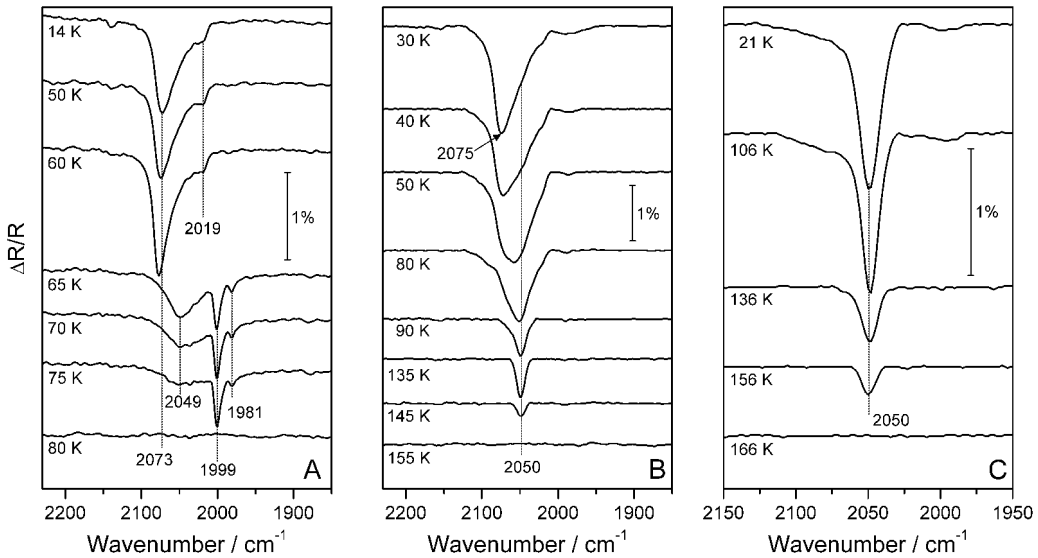

Fig. 17 RAIR spectra showing the changes to the OCS CO band following the sequential heating of (A) 100 L of pure OCS ice, (B) 100 L OCS deposited on 100 L of ASW and (C) 100 L of a 12% OCS : H_2O mixed ice. The annealing temperatures are shown in each figure.

intensity of the OCS multilayer feature. The change in profile of the OCS multilayer is assigned to the heterogeneity of the ASW film, in addition to the redistribution of the initial OCS coverage between desorption from the ASW surface and OCS trapped within the pores of the ASW film. The trapped OCS TPD peak observed in trace B corresponds to OCS released during the ASW–CI phase transition (trace E). Volcano desorption has been observed in the TPD spectra of many layered binary ice systems (where ASW is deposited underneath or on top of the more volatile ice) and is often independent of the adsorbate.[48,54,60,63,65–68] This high temperature feature demonstrates the ability of porous ASW to control the desorption of the vast majority of astrophysically relevant molecules, with similar behaviour being observed for CO_2,[60,63,67,68] CO,[48,63,65–67] Ar,[60,61,63,65] N_2,[65,67] O_2,[65] CH_4[60,65] and C_2H_5OH.[69]

The extent to which ASW can trap astrophysically relevant molecules within its porous structure during pore collapse can be demonstrated by additional experiments using crystalline ice. Crystalline H_2O has a much denser structure than ASW, with a much reduced surface area, hence decreasing the entrapment of molecules within the surface pores. The crystalline ice films in these experiments were formed by annealing an ASW film to a temperature corresponding to the ASW–CI transition for 3 minutes and re-cooling back to 14 K. Adsorption of OCS on CI is shown in Fig. 15C. It is clear that OCS desorption at the ASW–CI transition is totally blocked when OCS is deposited on CI, giving rise to a TPD profile similar to that observed when OCS is deposited directly on HOPG (trace A).

4.3.3 OCS : H_2O ice mixtures

TPD data. In contrast to the significant changes observed in the desorption profiles of sequentially and co-deposited CH_3OH and H_2O ices, the desorption of OCS from OCS : H_2O mixtures closely resembles that of OCS/H_2O binary ices. Desorption of OCS from a 100 L exposure of OCS : H_2O ice is shown in Fig. 15 (trace D). OCS desorption from the mixed ice is dominated by a sharp desorption feature at 158 K, which is almost identical to that observed for the OCS/H_2O ice, assigned to volcano desorption. However there are some differences in the desorption behaviour of OCS from the mixed ices when compared to the layered systems. Firstly, there is almost no "pure" OCS desorption from the mixed ice, in agreement with previous studies.[67] Instead, OCS desorption from the mixture is characterised by a very broad low intensity desorption feature first observed at around 106 K (Fig. 15 trace D inset). Secondly there is a clear enhancement of the co-desorption feature in the mixtures, which is negligible in the layered ices. These two observations suggest that OCS does not diffuse through the ASW ice when co-deposited as a mixture but remains trapped within the ice until the ASW–CI transition. This is in contrast to the desorption behaviour of other smaller astrophysically relevant molecules, such as CO and CO_2,[48,60,63,65–67] which are observed to diffuse through ASW at temperatures approximating the sublimation temperature of the pure ices, and suggests that molecular size plays an important role in the diffusion mechanism.

RAIRS: adsorption and desorption of OCS : H_2O mixed ices on HOPG. The position and profile of the OCS CO band within a OCS : H_2O mixed ice is modified when compared to pure OCS and OCS deposited on ASW. The CO band exhibits a much sharper peak for the mixed ice, coupled with an increased peak intensity, compared to OCS ices deposited on top of ASW films. This may suggest that the OCS adopts a more ordered orientation within the ASW ice. Furthermore the CO stretch at 2050 cm^{-1} in the mixture is downshifted by $\sim$11 cm^{-1} compared to an equivalent dose of OCS deposited on ASW, in good agreement with previous infrared studies of OCS : H_2O ice mixtures[205] and OCS within Ar and N_2 matrices.[212] The fact that the OCS band is only slightly

perturbed from the pure ice and is observed at a similar wavenumber when embedded within Ar and N_2 matrices, suggests that the interaction between OCS and H_2O is a weak one. This is further supported by the unperturbed infrared features of H_2O in the mixed ice which are identical to those seen for pure H_2O ices.

RAIR spectra showing the changes in the CO band of OCS during annealing of an OCS : H_2O ice mixture are shown in Fig. 17C. The changes to the CO infrared band during annealing can be explained by comparison with the TPD data shown in Fig. 15 and by the behaviour of the H_2O ν(OH) band during annealing (not shown). The minor changes in the CO band at 106 K in the RAIRS are consistent with the onset of OCS desorption from the mixed ice (Fig. 15D). The significant decrease in CO band intensity at 136 K in the RAIR spectrum coincides with the ASW–CI phase transition observed in the ν(OH) stretching region of H_2O[52] and is therefore associated with the release of OCS from the H_2O ice *via* volcano desorption. OCS is retained in the ice to slightly higher temperatures in the mixtures compared to the layered ice configuration (Fig. 17B), as observed for CH_3OH : H_2O ices. This is clearly shown by the presence of the CO feature in the RAIR spectrum beyond temperatures corresponding to the H_2O ASW–CI phase transition.

The RAIRS and TPD data obtained for all three OCS ice systems clearly show that H_2O significantly modifies the thermal desorption properties of OCS ices. However, it is also clear that although the thermal desorption of OCS exhibits similar trends to those observed for CH_3OH desorption from ASW ices, and for the desorption of more volatile species such as CO there are important differences.

The thermal behaviour of OCS for both OCS/H_2O and OCS : H_2O ices is clearly dominated by explosive volcano desorption, characteristic of all astrophysically relevant molecules. However negligible co-desorption with CI ice is observed, which implies that OCS cannot diffuse through H_2O ice and is simply trapped in the H_2O ice matrix. The absence of co-desorption could be a result of a weaker interaction between OCS and H_2O compared to CH_3OH and H_2O, which exhibits co-desorption features. However molecular size could also be a factor. Smaller, more volatile molecules, such as CO and N_2 exhibit co-desorption features in TPD (Fig. 4). The larger size of OCS could prevent it penetrating as deeply as smaller molecules into the ASW hydrogen-bonded network during the re-ordering of H_2O, thus preventing entrapment beyond the ASW–CI phase transition.

5. Desorption under astrophysical conditions

Desorption parameters calculated from TPD data can be incorporated into astrophysical models in order to determine desorption temperatures on an astronomical timescale as well as the residence times of the molecules as ices.[55] However, the desorption temperatures obtained from the kinetic data (Tables 1–3) cannot be directly incorporated into astrophysical models. This is because desorption is a non-equilibrium process that depends on the rate at which the ice is heated. Typical heating rates of icy mantles in hot cores are of the order of 1 K century^{-1},[43,70] clearly impractical under laboratory conditions. Furthermore, desorption also depends on the ice thickness for non-zero-order desorption.

To determine the extent to which the desorption temperature varies with heating rate, the desorption of pure ices adsorbed on HOPG has been simulated using a method developed by Collings *et al.*[48] Briefly, the method calculates the rate of change of gas phase concentration of the desorbing species as a function of temperature using the desorption order, desorption energy and pre-exponential factor extracted from the TPD data. The desorption includes two steps. The first step describes the rate of desorption of the ice from the surface, while the second step incorporates the rate of pumping of the gas from the apparatus, hence generating desorption curves that resemble TPD traces. For a more detailed description of the method, the reader is referred to Collings *et al.*[48] and Brown and Bolina.[55]

Fig. 18 shows simulated TPD traces for pure CH_3OH (Fig. 18A) and pure OCS (Fig. 18B) ices adsorbed on HOPG using heating rates ranging from those typically applied in the laboratory (0.5 K s^{-1}) to those determined for hot cores (1 K century^{-1}). The initial thickness of the ice in these simulations was 9.5×10^{21} molecules m^{-2}, corresponding to an ice thickness comparable to that of interstellar ices (0.3 μm).[67] Clearly the desorption temperature of the ice decreases markedly, as the heating rate decreases. The desorption temperature for CH_3OH ranges from 171 K at a 0.5 K s^{-1} heating rate, down to 101 K at an astrophysical heating rate of 1 K century^{-1}. A similar reduction in desorption temperature is also seen for OCS, H_2O,[55] NH_3,[55] C_2H_5OH, and CO_2 with data summarised in Table 4.

Using this model, the effects of varying the ice thickness on the desorption temperature were also investigated for pure CH_3OH and OCS ices adsorbed on HOPG. These simulations used a constant heating rate of 1 K century^{-1} and the kinetic parameters listed in Table 3. Fig. 18C and D show that the desorption temperature increases with ice thickness as expected. It is also evident that for systems exhibiting fractional-order desorption, the desorption traces for different ice thicknesses cannot be simply overlaid. This is more marked for CH_3OH ices (Fig. 18C) which exhibit a greater deviation from zero-order kinetics than OCS (Fig. 5D), with desorption orders of 0.35 and 0.11 respectively. This is in contrast to species that exhibit perfect zero-order desorption, where the desorption profiles of varying thickness can be overlaid for a given heating rate.[67] This result demonstrates the importance of using accurately determined kinetic parameters in astrophysical models.

6. Summary and future work

Detailed surface science investigations from a range of groups, including our own, have shown that the desorption of interstellar ices is not instantaneous, and that the composition and morphology of the ice affects its adsorption and desorption markedly. Initial studies[67] allowed the broad classification of molecules according to their desorption properties and more detailed studies[46,47,50–52,55,57,69,177] have now allowed the accurate determination of desorption kinetics for certain model interstellar ices. These numbers can then be incorporated

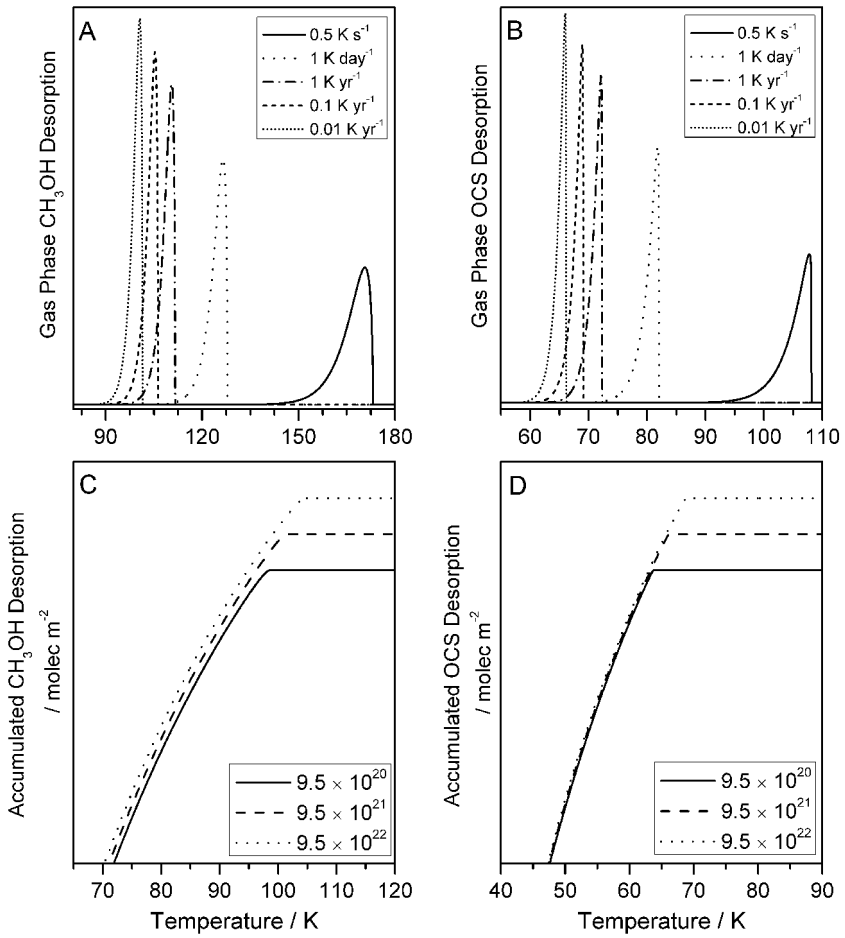

Fig. 18 Simulated TPD desorption profiles for (A) pure CH_3OH ice and (B) pure OCS ice from HOPG as a function of heating rate. The TPD curves were generated using the kinetic parameters listed in Table 3. The thickness of the ice is of the order of 0.3 μm, corresponding to an initial surface coverage of 9.5×10^{21} molecules m^{-2}. The figure also shows the cumulative desorption of (C) CH_3OH and (D) OCS into the gas phase as a function of ice thickness at a heating rate of 0.01 K y^{-1}. The ice coverages are shown in the figure.

Table 4 Table showing the desorption temperatures for pure molecular ices adsorbed on HOPG as a function of heating rate. The initial thickness of the ice was set to 9.5×10^{21} molecules m^{-2}

	Desorption temperature/K				
	Heating rate				
Molecule	1 K century^{-1}	0.1 K y^{-1}	1 K y^{-1}	1 K day^{-1}	0.5 K s^{-1}
NH_3	64	67	71	82	113[a]
CH_3OH	101	105	111	126	171
H_2O	103	109	114	132	182
C_2H_5OH	110	114	118	131	163
CO_2	61	64	68	80	118
OCS	66	69	72	82	108

[a] A 0.2 K s^{-1} heating rate was applied to NH_3 ices.

into accurate models of desorption on astrophysically relevant timescales.[55]

Despite the clear advances in our understanding of the adsorption and desorption of model interstellar ices from dust grain analogue surfaces, a large amount of work remains to be done in order to enable a complete understanding of molecular ices in the ISM. In particular, most studies to date have focussed on binary ices, consisting of only two components. Real interstellar ices contain many different species and hence studies of more complex ices are required. The importance of this has been highlighted by recent studies in our laboratory[213] where the desorption of OCS was found to be different when adsorbed on CH_3OH : H_2O ices compared to on pure ASW ice or in a mixed OCS : H_2O ice. Further studies of the role of the underlying grain surface are also necessary, as shown by recent work on the desorption of CH_3OH from a range of model dust grain surfaces.[177] In particular, studies of more porous and defective surfaces, such as those which are likely to be found in the ISM, are also important as surface porosity has been shown to strongly influence the desorption kinetics of C_6H_6 from a porous silica model grain surface.[214] In addition to these studies of adsorption and desorption, further detailed studies of molecular formation on a range of model dust grain surfaces are also required. Further detailed and accurate studies, under UHV conditions, of the effects of non-thermal processing (induced by UV light, cosmic rays, and energetic ion bombardment) on interstellar ices will also aid our understanding of interstellar chemistry and enhance our knowledge of the origin of stars and planets.

Acknowledgements

The Leverhulme Trust are thanked for a post-doctoral fellowship for DJB and the EPSRC are acknowledged for funding the earlier work (on CH_3OH, H_2O and NH_3) described in this perspective. The work in our group that has been summarised in this article has been undertaken by several people over a number of years, in addition to the authors. A. S. Bolina, A. J. Wolff, C. Carlstedt, J. L. Edridge, K. Freimann and S. Belbin are acknowledged for their contributions to the data reported here. M. R. S. McCoustra and M. P. Collings are also acknowledged for fruitful discussions and collaborations.

References

1 http://astrochemistry.net.
2 E. Herbst and E. F. van Dishoeck, *Annu. Rev. Astron. Astrophys.*, 2009, **47**, 427–480.
3 M. W. Werner and M. Harwit, *Astrophys. J.*, 1968, **154**, 881–889.
4 G. R. Carruthers, *Astrophys. J.*, 1970, **161**, L81–L85.
5 R. W. Wilson, K. B. Jefferts and A. A. Penzias, *Astrophys. J.*, 1970, **161**, L43–L44.
6 M. B. Bell, P. A. Feldman, J. K. G. Watson, M. C. McCarthy, M. J. Travers, C. A. Gottlieb and P. Thaddeus, *Astrophys. J.*, 1999, **518**, 740–747.
7 G. A. Blake, E. C. Sutton, C. R. Masson and T. G. Phillips, *Astrophys. J.*, 1987, **315**, 621–645.
8 B. E. Turner, *Astrophys. J., Suppl. Ser.*, 1991, **76**, 617–686.
9 R. J. Gould and E. E. Salpeter, *Astrophys. J.*, 1963, **138**, 393–407.
10 D. Hollenbach and E. E. Salpeter, *Astrophys. J.*, 1971, **163**, 155–164.
11 T. A. Pauls, T. L. Wilson, J. H. Bieging and R. N. Martin, *Astron. Astrophys.*, 1983, **124**, 23–38.
12 K. M. Menten, C. M. Walmsley, C. Henkel and T. L. Wilson, *Astron. Astrophys.*, 1986, **157**, 318–328.
13 S. B. Charnley, M. E. Kress, A. G. G. M. Tielens and T. J. Millar, *Astrophys. J.*, 1995, **448**, 232–239.
14 W. D. Watson, *Rev. Mod. Phys.*, 1976, **48**, 513–552.
15 M. Allen and G. W. Robinson, *Astrophys. J.*, 1977, **212**, 396–415.
16 A. G. G. M. Tielens and W. Hagen, *Astron. Astrophys.*, 1982, **114**, 245–260.
17 L. B. d'Hendecourt, L. J. Allamandola and J. M. Greenberg, *Astron. Astrophys.*, 1985, **152**, 130–150.
18 P. D. Brown and S. B. Charnley, *Mon. Not. R. Astron. Soc.*, 1990, **244**, 432–443.
19 T. I. Hasegawa, E. Herbst and C. M. Leung, *Astrophys. J., Suppl. Ser.*, 1992, **82**, 167–195.
20 S. S. Prasad and S. P. Tarafdar, *Astrophys. J.*, 1983, **267**, 603–609.
21 J. M. Greenberg, *Astrophys. Space Sci.*, 1986, **128**, 17–31.
22 D. A. Williams and E. Herbst, *Surf. Sci.*, 2002, **500**, 823–837.
23 B. T. Draine, *Annu. Rev. Astron. Astrophys.*, 2003, **41**, 241–289.
24 J. S. Mathis, *Annu. Rev. Astron. Astrophys.*, 1990, **28**, 37–70.
25 L. J. Allamandola, M. P. Bernstein, S. A. Sandford and R. L. Walker, *Space Sci. Rev.*, 1999, **90**, 219–232.
26 S. A. Sandford, *Meteorit. Planet. Sci.*, 1996, **31**, 449–476.
27 A. G. G. M. Tielens, A. T. Tokunaga, T. R. Geballe and F. Baas, *Astrophys. J.*, 1991, **381**, 181–199.
28 D. C. B. Whittet, in *Dust and Chemistry in Astronomy*, ed. T. J. Millar and D. A. Williams, IOP Publishing Ltd, Bristol, 1993, pp. 9–36.
29 D. C. B. Whittet, *Dust in the Galactic Environment*, IOP Publishing Ltd, Bristol, 2nd edn, 2003.
30 P. Ehrenfreund, A. C. A. Boogert, P. A. Gerakines, A. G. G. M. Tielens and E. F. van Dishoeck, *Astron. Astrophys.*, 1997, **328**, 649–669.
31 P. Ehrenfreund, A. C. A. Boogert, P. A. Gerakines, D. J. Jansen, W. A. Schutte, A. G. G. M. Tielens and E. F. van Dishoeck, *Astron. Astrophys.*, 1996, **315**, L341–L344.
32 B. E. Turner, *Astrophys. J.*, 1990, **362**, L29–L33.
33 J. M. Greenberg, *Astrophys. Space Sci.*, 1976, **39**, 9–18.
34 M. P. Bernstein, S. A. Sandford, L. J. Allamandola, S. Chang and M. A. Scharberg, *Astrophys. J.*, 1995, **454**, 327–344.
35 M. H. Moore, B. Donn, R. Khanna and M. F. A'Hearn, *Icarus*, 1983, **54**, 388–405.
36 L. B. d'Hendecourt, L. J. Allamandola, R. J. A. Grim and J. M. Greenberg, *Astron. Astrophys.*, 1986, **158**, 119–134.
37 A. Schriver, L. Schriver-Mazzuoli, P. Ehrenfreund and L. d'Hendecourt, *Chem. Phys.*, 2007, **334**, 128–137.
38 R. L. Hudson and M. H. Moore, *Radiat. Phys. Chem.*, 1995, **45**, 779–789.
39 M. J. Loeffler, G. A. Baratta, M. E. Palumbo, G. Strazzulla and R. A. Baragiola, *Astron. Astrophys.*, 2005, **435**, 587–594.
40 M. E. Palumbo, *Astron. Astrophys.*, 2006, **453**, 903–909.
41 U. Raut, M. Fama, M. J. Loeffler and R. A. Baragiola, *Astrophys. J.*, 2008, **687**, 1070–1074.
42 S. B. Charnley, A. G. G. M. Tielens and T. J. Millar, *Astrophys. J.*, 1992, **399**, L71–L74.
43 S. Viti and D. A. Williams, *Mon. Not. R. Astron. Soc.*, 1999, **305**, 755–762.
44 K. Acharyya, G. W. Fuchs, H. J. Fraser, E. F. van Dishoeck and H. Linnartz, *Astron. Astrophys.*, 2007, **466**, 1005–1012.
45 G. W. Fuchs, K. Acharyya, S. E. Bisschop, K. I. Öberg, F. van Broekhuizen, H. J. Fraser, S. Schlemmer, E. F. van Dishoeck and H. Linnartz, *Faraday Discuss.*, 2006, **133**, 331–345.
46 A. J. Wolff, C. Carlstedt and W. A. Brown, *J. Phys. Chem. C*, 2007, **111**, 5990–5999.
47 H. J. Fraser, M. P. Collings, M. R. S. McCoustra and D. A. Williams, *Mon. Not. R. Astron. Soc.*, 2001, **327**, 1165–1172.
48 M. P. Collings, J. W. Dever, H. J. Fraser and M. R. S. McCoustra, *Astrophys. Space Sci.*, 2003, **285**, 633–659.
49 K. I. Öberg, F. van Broekhuizen, H. J. Fraser, S. E. Bisschop, E. F. van Dishoeck and S. Schlemmer, *Astrophys. J.*, 2005, **621**, L33–L36.
50 A. S. Bolina and W. A. Brown, *Surf. Sci.*, 2005, **598**, 45–56.
51 A. S. Bolina, A. J. Wolff and W. A. Brown, *J. Chem. Phys.*, 2005, **122**, 044713.
52 A. S. Bolina, A. J. Wolff and W. A. Brown, *J. Phys. Chem. B*, 2005, **109**, 16836–16845.
53 M. N. Mautner, V. Abdelsayed, M. S. El-Shall, J. D. Thrower, S. D. Green, M. P. Collings and M. R. S. McCoustra, *Faraday Discuss.*, 2006, **133**, 103–112.
54 O. Gálvez, I. K. Ortega, B. Maté, M. A. Moreno, B. Martín-Llorente, V. J. Herrero, R. Escribano and P. J. Gutiérrez, *Astron. Astrophys.*, 2007, **472**, 691–698.
55 W. A. Brown and A. S. Bolina, *Mon. Not. R. Astron. Soc.*, 2007, **374**, 1006–1014.
56 D. A. Williams, W. A. Brown, S. D. Price, J. M. C. Rawlings and S. Viti, *Astron. Geophys.*, 2007, **48**, 25–34.
57 D. J. Burke, A. J. Wolff, J. L. Edridge and W. A. Brown, *J. Chem. Phys.*, 2008, **128**, 104702.
58 A. Bar-Nun, G. Notesco and T. Owen, *Icarus*, 2007, **190**, 655–659.
59 J. A. Ghormley, *J. Chem. Phys.*, 1967, **46**, 1321–1325.
60 A. Bar-Nun, G. Herman, D. Laufer and M. L. Rappaport, *Icarus*, 1985, **63**, 317–332.
61 D. Laufer, E. Kochavi and A. Bar-Nun, *Phys. Rev. B: Condens. Matter*, 1987, **36**, 9219–9227.
62 A. Bar-Nun, I. Kleinfeld and E. Kochavi, *Phys. Rev. B: Condens. Matter*, 1988, **38**, 7749–7754.
63 R. L. Hudson and B. Donn, *Icarus*, 1991, **94**, 326–332.
64 G. Notesco and A. Bar-Nun, *Icarus*, 1997, **126**, 336–341.
65 P. Ayotte, R. S. Smith, K. P. Stevenson, Z. Dohnálek, G. A. Kimmel and B. D. Kay, *J. Geophys. Res. Planets*, 2001, **106**, 33387–33392.
66 M. P. Collings, J. W. Dever, H. J. Fraser, M. R. S. McCoustra and D. A. Williams, *Astrophys. J.*, 2003, **583**, 1058–1062.
67 M. P. Collings, M. A. Anderson, R. Chen, J. W. Dever, S. Viti, D. A. Williams and M. R. S. McCoustra, *Mon. Not. R. Astron. Soc.*, 2004, **354**, 1133–1140.
68 S. Malyk, G. Kumi, H. Reisler and C. Wittig, *J. Phys. Chem. A*, 2007, **111**, 13365–13370.
69 D. J. Burke, A. J. Wolff, J. L. Edridge and W. A. Brown, *Phys. Chem. Chem. Phys.*, 2008, **10**, 4956–4967.
70 S. Viti, M. P. Collings, J. W. Dever, M. R. S. McCoustra and D. A. Williams, *Mon. Not. R. Astron. Soc.*, 2004, **354**, 1141–1145.

71 R. T. Garrod and E. Herbst, *Astron. Astrophys.*, 2006, **457**, 927–936.
72 S. A. Sandford and L. J. Allamandola, *Icarus*, 1990, **87**, 188–192.
73 S. A. Sandford and L. J. Allamandola, *Icarus*, 1988, **76**, 201–224.
74 E. Dartois, *Space Sci. Rev.*, 2005, **119**, 293–310.
75 E. L. Gibb, D. C. B. Whittet, A. C. A. Boogert and A. G. G. M. Tielens, *Astrophys. J., Suppl. Ser.*, 2004, **151**, 35–73.
76 E. L. Gibb, D. C. B. Whittet, W. A. Schutte, A. C. A. Boogert, J. E. Chiar, P. Ehrenfreund, P. A. Gerakines, J. V. Keane, A. G. G. M. Tielens, E. F. van Dishoeck and O. Kerkhof, *Astrophys. J.*, 2000, **536**, 347–356.
77 T. P. Stecher, *Astrophys. J.*, 1965, **142**, 1683–1684.
78 T. P. Stecher and B. Donn, *Astrophys. J.*, 1965, **142**, 1681–1683.
79 J. S. Mathis, *Astrophys. J.*, 1994, **422**, 176–186.
80 L. J. Allamandola, S. A. Sandford, A. G. G. M. Tielens and T. M. Herbst, *Astrophys. J.*, 1992, **399**, 134–146.
81 E. Bussoletti, L. Colangeli and V. Orofino, *Astrophys. J.*, 1987, **321**, L87–L90.
82 W. W. Duley and D. A. Williams, *Mon. Not. R. Astron. Soc.*, 1983, **205**, 67–70.
83 R. Papoular, J. Conard, O. Guillois, I. Nenner, C. Reynaud and J.-N. Rouzaud, *Astron. Astrophys.*, 1996, **315**, 222–236.
84 A. Li and B. T. Draine, *Astrophys. J.*, 2001, **554**, 778–802.
85 S. A. Sandford, L. J. Allamandola, A. G. G. M. Tielens, K. Sellgren, M. Tapia and Y. Pendleton, *Astrophys. J.*, 1991, **371**, 607–620.
86 J. M. Greenberg, A. Li, C. X. Mendoza-Gómez, W. A. Schutte, P. A. Gerakines and M. de Groot, *Astrophys. J.*, 1995, **455**, L177–L180.
87 P. A. Gerakines, W. A. Schutte, J. M. Greenberg and E. F. van Dishoeck, *Astron. Astrophys.*, 1995, **296**, 810–818.
88 L. J. Allamandola, S. A. Sandford and G. J. Valero, *Icarus*, 1988, **76**, 225–252.
89 P. Ehrenfreund and W. A. Schutte, *Adv. Space Res.*, 2000, **25**, 2177–2188.
90 P. Ehrenfreund and S. B. Charnley, *Annu. Rev. Astron. Astrophys.*, 2000, **38**, 427–483.
91 N. Boudin, W. A. Schutte and J. M. Greenberg, *Astron. Astrophys.*, 1998, **331**, 749–759.
92 S. A. Sandford, L. J. Allamandola, A. G. G. M. Tielens and G. J. Valero, *Astrophys. J.*, 1988, **329**, 498–510.
93 G. Vidali, V. Pirronello, L. Li, J. Roser, G. Manicò, E. Congiu, H. Mehl, A. Lederhendler, H. B. Perets, J. R. Brucato and O. Biham, *J. Phys. Chem. A*, 2007, **111**, 12611–12619.
94 V. Pirronello, O. Biham, C. Liu, L. Shen and G. Vidali, *Astrophys. J.*, 1997, **483**, L131–L134.
95 V. Pirronello, C. Liu, J. E. Roser and G. Vidali, *Astron. Astrophys.*, 1999, **344**, 681–686.
96 V. Mennella, *Astrophys. J.*, 2008, **684**, L25–L28.
97 H. J. Fraser, S. E. Bisschop, K. M. Pontoppidan, A. G. G. M. Tielens and E. F. van Dishoeck, *Mon. Not. R. Astron. Soc.*, 2005, **356**, 1283–1292.
98 J. Goering, S. Sah, U. Burghaus and K. W. Street Jr, *Surf. Interface Anal.*, 2008, **40**, 1423–1429.
99 L. Hornekær, A. Baurichter, V. V. Petrunin, D. Field and A. C. Luntz, *Science*, 2003, **302**, 1943–1946.
100 G. Manicò, G. Raguní, V. Pirronello, J. E. Roser and G. Vidali, *Astrophys. J.*, 2001, **548**, L253–L256.
101 J. E. Roser, G. Manicò, V. Pirronello and G. Vidali, *Astrophys. J.*, 2002, **581**, 276–284.
102 S. C. Creighan, J. S. A. Perry and S. D. Price, *J. Chem. Phys.*, 2006, **124**, 114701.
103 J. E. Roser, G. Vidali, G. Manicò and V. Pirronello, *Astrophys. J.*, 2001, **555**, L61–L64.
104 S. Ioppolo, H. M. Cuppen, C. Romanzin, E. F. van Dishoeck and H. Linnartz, *Astrophys. J.*, 2008, **686**, 1474–1479.
105 N. Miyauchi, H. Hidaka, T. Chigai, A. Nagaoka, N. Watanabe and A. Kouchi, *Chem. Phys. Lett.*, 2008, **456**, 27–30.
106 H. Mokrane, H. Chaabouni, M. Accolia, E. Congiu, F. Dulieu, M. Chehrouri and J. L. Lemaire, *Astrophys. J. Lett.*, 2009, **705**, L195–L198.
107 N. Watanabe and A. Kouchi, *Astrophys. J.*, 2002, **571**, L173–L176.
108 N. Watanabe, T. Shiraki and A. Kouchi, *Astrophys. J.*, 2003, **588**, L121–L124.
109 N. Watanabe, A. Nagaoka, T. Shiraki and A. Kouchi, *Astrophys. J.*, 2004, **616**, 638–642.
110 K. Hiraoka, N. Ohashi, Y. Kihara, K. Yamamoto, T. Sato and A. Yamashita, *Chem. Phys. Lett.*, 1994, **229**, 408–414.
111 H. Hidaka, A. Kouchi and N. Watanabe, *J. Chem. Phys.*, 2007, **126**, 204707.
112 G. W. Fuchs, H. M. Cuppen, S. Ioppolo, C. Romanzin, S. E. Bisschop, S. Andersson, E. F. van Dishoeck and H. Linnartz, *Astron. Astrophys.*, 2009, **505**, 629–639.
113 G. Vidali, L. Ling, J. E. Roser and R. Badman, *Adv. Space Res.*, 2009, **43**, 1291–1298.
114 G. Vidali, J. E. Roser, L. Ling, E. Congiu, G. Manicò and V. Pirronello, *Faraday Discuss.*, 2006, **133**, 125–135.
115 G. Vidali, J. E. Roser, G. Manicò and V. Pirronello, *Adv. Space Res.*, 2004, **33**, 6–13.
116 N. Watanabe and A. Kouchi, *Prog. Surf. Sci.*, 2008, **83**, 439–489.
117 J. Klinger, *J. Phys. Chem.*, 1983, **87**, 4209–4214.
118 H. Patashnick, G. Rupprecht and D. W. Schuerman, *Nature*, 1974, **250**, 313–314.
119 F. L. Whipple, *Astrophys. J.*, 1950, **111**, 375–394.
120 R. Smoluchowski, *Science*, 1978, **201**, 809–811.
121 G. Kumi, S. Malyk, S. Hawkins, H. Reisler and C. Wittig, *J. Phys. Chem. A*, 2006, **110**, 2097–2105.
122 A. Bar-Nun, J. Dror, E. Kochavi and D. Laufer, *Phys. Rev. B: Condens. Matter*, 1987, **35**, 2427–2435.
123 A. Bar-Nun and I. Kleinfeld, *Icarus*, 1989, **80**, 243–253.
124 E. Mayer and R. Pletzer, *Nature*, 1986, **319**, 298–301.
125 K. P. Stevenson, G. A. Kimmel, Z. Dohnálek, R. S. Smith and B. D. Kay, *Science*, 1999, **283**, 1505–1507.
126 C. Martin, C. Manca and P. Roubin, *Surf. Sci.*, 2002, **502–503**, 275–279.
127 G. A. Kimmel, K. P. Stevenson, Z. Dohnálek, R. S. Smith and B. D. Kay, *J. Chem. Phys.*, 2001, **114**, 5284–5294.
128 A. Kouchi, T. Yamamoto, T. Kozasa, T. Kuroda and J. M. Greenberg, *Astron. Astrophys.*, 1994, **290**, 1009–1018.
129 P. Jenniskens and D. F. Blake, *Science*, 1994, **265**, 753–756.
130 J. Klinger, *Icarus*, 1981, **47**, 320–324.
131 R. Smoluchowski, *Astrophys. J.*, 1981, **244**, L31–L34.
132 R. Smoluchowski, *Science*, 1983, **222**, 161–163.
133 P. Jenniskens, D. F. Blake, M. A. Wilson and A. Pohorille, *Astrophys. J.*, 1995, **455**, 389–401.
134 A. H. Narten, C. G. Venkatesh and S. A. Rice, *J. Chem. Phys.*, 1976, **64**, 1106–1121.
135 R. S. Smith and B. D. Kay, *Nature*, 1999, **398**, 788–791.
136 R. S. Smith, Z. Dohnálek, G. A. Kimmel, K. P. Stevenson and B. D. Kay, *Chem. Phys.*, 2000, **258**, 291–305.
137 R. S. Smith, C. Huang, E. K. L. Wong and B. D. Kay, *Phys. Rev. Lett.*, 1997, **79**, 909–912.
138 A. Omont, S. H. Moseley, T. Forveille, W. J. Glaccum, P. M. Harvey, L. Likkel, R. F. Loewenstein and C. M. Lisse, *Astrophys. J.*, 1990, **355**, L27–L30.
139 D. C. Jewitt and J. Luu, *Nature*, 2004, **432**, 731–733.
140 F. Merlin, A. Guilbert, C. Dumas, M. A. Barucci, C. de Bergh and P. Vernazza, *Astron. Astrophys.*, 2007, **466**, 1185–1188.
141 P. Jenniskens and D. F. Blake, *Astrophys. J.*, 1996, **473**, 1104–1113.
142 E. Vichnevetski, A. D. Bass and L. Sanche, *J. Chem. Phys.*, 2000, **113**, 3874–3881.
143 B. Rowland, M. Fisher and J. P. Devlin, *J. Chem. Phys.*, 1991, **95**, 1378–1384.
144 H. G. Hixson, M. J. Wojcik, M. S. Devlin and J. P. Devlin, *J. Chem. Phys.*, 1992, **97**, 753–767.
145 N. Horimoto, H. S. Kato and M. Kawai, *J. Chem. Phys.*, 2002, **116**, 4375–4378.
146 L. Amiaud, J. H. Fillion, S. Baouche, F. Dulieu, A. Momeni and J. L. Lemaire, *J. Chem. Phys.*, 2006, **124**, 094702.
147 J. P. Devlin and V. Buch, *J. Phys. Chem.*, 1995, **99**, 16534–16548.
148 V. Buch and J. P. Devlin, *J. Chem. Phys.*, 1991, **94**, 4091–4092.
149 H. J. Fraser, M. P. Collings, J. W. Dever and M. R. S. McCoustra, *Mon. Not. R. Astron. Soc.*, 2004, **353**, 59–68.
150 N. Watanabe and A. Kouchi, *Astrophys. J.*, 2002, **567**, 651–655.
151 G. M. Muñoz Caro and W. A. Schutte, *Astron. Astrophys.*, 2003, **412**, 121–132.
152 W. A. Schutte, A. C. A. Boogert, A. G. G. M. Tielens, D. C. B. Whittet, P. A. Gerakines, J. E. Chiar, P. Ehrenfreund,

J. M. Greenberg, E. F. van Dishoeck and T. de Graauw, *Astron. Astrophys.*, 1999, **343**, 966–976.
153 J. D. Thrower, D. J. Burke, M. P. Collings, A. Dawes, P. D. Holtom, F. Jamme, P. Kendall, W. A. Brown, I. P. Clark, H. J. Fraser, M. R. S. McCoustra, N. J. Mason and A. W. Parker, *Astrophys. J.*, 2008, **673**, 1233–1239.
154 R. L. Hudson and M. H. Moore, *Icarus*, 1999, **140**, 451–461.
155 M. P. Collings, J. W. Dever and M. R. S. McCoustra, *Chem. Phys. Lett.*, 2005, **415**, 40–45.
156 H. J. Fraser, M. P. Collings and M. R. S. McCoustra, *Rev. Sci. Instrum.*, 2002, **73**, 2161–2170.
157 S. A. Sandford and L. J. Allamandola, *Astrophys. J.*, 1993, **417**, 815–825.
158 S. A. Sandford and L. J. Allamandola, *Astrophys. J.*, 1990, **355**, 357–372.
159 S. A. Sandford and L. J. Allamandola, *Icarus*, 1993, **106**, 478–488.
160 S. A. Sandford and L. J. Allamandola, *Astrophys. J.*, 1993, **409**, L65–L68.
161 G. Notesco and A. Bar-Nun, *Icarus*, 2000, **148**, 456–463.
162 G. Notesco, A. Bar-Nun and T. Owen, *Icarus*, 2003, **162**, 183–189.
163 L. Hornekær, Šljivancanin, W. Xu, R. Otero, E. Rauls, I. Stensgaard, E. Lægsgaard, B. Hammer and F. Besenbacher, *Phys. Rev. Lett.*, 2006, **96**, 156104.
164 D. A. Adriaens, T. P. M. Goumans, C. R. A. Catlow and W. A. Brown, *J. Phys. Chem. C*, 2010, **114**, 1892–1900.
165 T. Fromherz, C. Mendoza and F. Ruette, *Mon. Not. R. Astron. Soc.*, 1993, **263**, 851–860.
166 S. Klose, *Astron. Astrophys.*, 1992, **260**, 321–328.
167 F. O. Gordon, *Astrophys. J.*, 1978, **266**, 87–94.
168 X. Sha and B. Jackson, *Surf. Sci.*, 2002, **496**, 318–330.
169 P. A. Gerakines, M. H. Moore and R. L. Hudson, *Icarus*, 2004, **170**, 202–213.
170 P. A. Gerakines, W. A. Schutte and P. Ehrenfreund, *Astron. Astrophys.*, 1996, **312**, 289–305.
171 P. A. Gerakines, M. H. Moore and R. L. Hudson, *Astron. Astrophys.*, 2000, **357**, 793–800.
172 A. Wada, N. Mochizuki and K. Hiraoka, *Astrophys. J.*, 2006, **644**, 300–306.
173 C. J. Bennett and R. I. Kaiser, *Astrophys. J.*, 2007, **661**, 899–909.
174 R. I. Kaiser and K. Roessler, *Astrophys. J.*, 1998, **503**, 959–975.
175 M. H. Moore and R. L. Hudson, *Icarus*, 2000, **145**, 282–288.
176 D. P. P. Andrade, H. M. Boechat-Roberty, R. Martinez, M. G. P. Homem, E. F. da Silveira and M. L. M. Rocco, *Surf. Sci.*, 2009, **603**, 1190–1196.
177 S. D. Green, A. S. Bolina, R. Chen, M. P. Collings, W. A. Brown and M. R. S. McCoustra, *Mon. Not. R. Astron. Soc.*, 2009, **398**, 357–367.
178 H. Ulbricht, R. Zacharia, N. Cindir and T. Hertel, *Carbon*, 2006, **44**, 2931–2942.
179 S. Y. Nishimura, R. F. Gibbons and N. J. Tro, *J. Phys. Chem. B*, 1998, **102**, 6831–6834.
180 A. M. de Jong and J. W. Niemantsverdriet, *Surf. Sci.*, 1990, **233**, 355–365.
181 D. A. King, *Surf. Sci.*, 1975, **384**, 384–402.
182 L. Hornekær, A. Baurichter, V. V. Petrunin, A. C. Luntz, B. D. Kay and A. Al-Halabi, *J. Chem. Phys.*, 2005, **122**, 124701.
183 J. Elsila, L. J. Allamandola and S. A. Sandford, *Astrophys. J.*, 1997, **479**, 818–838.
184 E. Dartois, K. Demyk, L. d'Hendecourt and P. Ehrenfreund, *Astron. Astrophys.*, 1999, **351**, 1066–1074.
185 P. Ehrenfreund, O. Kerkhof, W. A. Schutte, A. C. A. Boogert, P. A. Gerakines, E. Dartois, L. d'Hendecourt, A. G. G. M. Tielens, E. F. van Dishoeck and D. C. B. Whittet, *Astron. Astrophys.*, 1999, **350**, 240–253.
186 R. Souda, *Phys. Rev. B: Condens. Matter*, 2007, **75**, 184116.
187 D. F. Blake, L. J. Allamandola, S. A. Sandford, D. Huggins and F. Freund, *Science*, 1991, **254**, 548–551.
188 R. J. A. Grim, F. Baas, T. R. Geballe, J. M. Greenberg and W. A. Schutte, *Astron. Astrophys.*, 1991, **243**, 473–477.
189 L. J. Allamandola, S. A. Sandford, A. G. G. M. Tielens and T. M. Herbst, *Astrophys. J.*, 1992, **399**, 134–146.
190 C. J. Skinner, A. G. G. M. Tielens, M. J. Barlow and K. Justtanont, *Astrophys. J.*, 1992, **399**, L79–L82.
191 R. L. Hudson and M. H. Moore, *Astrophys. J.*, 1993, **409**, L29–L32.
192 K. M. Pontoppidan, E. Dartois, E. F. van Dishoeck, W.-F. Thi and L. d'Hendecourt, *Astron. Astrophys.*, 2003, **404**, L17–L20.
193 E. Dartois, W. A. Schutte, T. R. Geballe, K. Demyk, P. Ehrenfreund and L. d'Hendecourt, *Astron. Astrophys.*, 1999, **342**, L32–L35.
194 P. Ehrenfreund, E. Dartois, K. Demyk and L. d'Hendecourt, *Astron. Astrophys.*, 1998, **339**, L17–L20.
195 R. S. Smith and B. D. Kay, *Surf. Rev. Lett.*, 1997, **4**, 781–797.
196 R. Souda, *Phys. Rev. Lett.*, 2004, **93**, 235502.
197 R. Souda, H. Kawanowa, M. Kondo and Y. Gotoh, *J. Chem. Phys.*, 2003, **119**, 6194–6200.
198 R. Souda, *J. Chem. Phys.*, 2005, **122**, 134711.
199 R. Souda, *J. Chem. Phys.*, 2004, **121**, 8676–8679.
200 P. A. Thiel and T. E. Madey, *Surf. Sci. Rep.*, 1987, **7**, 211–385.
201 E. H. G. Backus, M. L. Grecea, A. W. Kleyn and M. Bonn, *Phys. Rev. Lett.*, 2004, **92**, 236101.
202 E. Marcq, B. Bézard, T. Encrenaz and M. Birlan, *Icarus*, 2005, **179**, 375–386.
203 M. J. Mumma, M. A. DiSanti, N. Dello Russo, K. Magee-Sauer, E. Gibb and R. Novak, *Adv. Space Res.*, 2003, **31**, 2563–2575.
204 S. B. Charnley, P. Ehrenfreund and Y.-J. Kuan, *Spectrochim. Acta, Part A*, 2001, **57**, 685–704.
205 M. E. Palumbo, A. G. G. M. Tielens and A. T. Tokunaga, *Astrophys. J.*, 1995, **449**, 674–680.
206 M. E. Palumbo, T. R. Geballe and A. G. G. M. Tielens, *Astrophys. J.*, 1997, **479**, 839–844.
207 D. S. Hudgins, S. A. Sandford, L. J. Allamandola and A. G. G. M. Tielens, *Astrophys. J., Suppl. Ser.*, 1993, **86**, 713–870.
208 J. Hatchell, M. A. Thompson, T. J. Millar and G. H. Macdonald, *Astron. Astrophys.*, 1998, **338**, 713–722.
209 S. B. Charnley, *Astrophys. J.*, 1997, **481**, 396–405.
210 T. R. Geballe, F. Baas, J. M. Greenberg and W. A. Schutte, *Astron. Astrophys.*, 1985, **146**, L6–L8.
211 R. F. Ferrante, M. H. Moore, M. M. Spiliotis and R. L. Hudson, *Astron. Astrophys.*, 2008, **684**, 1210–1220.
212 V. I. Lang and J. S. Winn, *J. Chem. Phys.*, 1991, **94**, 5270–5274.
213 D. J. Burke, S. Belbin and W. A. Brown, in preparation.
214 J. D. Thrower, M. P. Collings, F. J. M. Rutten and M. R. S. McCoustra, *Mon. Not. R. Astron. Soc.*, 2009, **394**, 1510–1518.